Stamm, F. M., Zambardi, T., Chmeleff, J., Schott, J., von Blanckenburg, F., Oelkers, E. H. (2019): The experimental determination of equilibrium Si isotope fractionation factors among H4SiO4°, H3SiO4− and amorphous silica (SiO2·0.32 H2O) at 25 and 75°C using the three-isotope method. - Geochimica et Cosmochimica Acta, 255, 49-68.

https://doi.org/10.1016/j.gca.2019.03.035

THE EXPERIMENTAL DETERMINATION OF EQUILIBRIUM Si ISOTOPE FRACTIONATION FACTORS AMONG $H_4SiO_4^\circ$, $H_3SiO_4^-$ AND AMORPHOUS SILICA ($SiO_2 \cdot 0.32\ H_2O$) AT 25 AND 75 ^{O}C USING THE THREE-ISOTOPE METHOD

Franziska M. Stamm[a], Thomas Zambardi[b], Jérôme Chmeleff[a], Jacques Schott[a], Friedhelm von Blanckenburg[c], Eric H. Oelkers[a,d]

a Géosciences Environnement Toulouse, CNRS-UPS-OMP, 14 av. Édouard Belin, 31400 Toulouse, France

b LEGOS, Laboratoire d'Etudes en Géophysique et Océanographie Spatiales (CNRS/UPS/CNES/IRD), Observatoire Midi-Pyrénées14 Avenue Edouard Belin, 31400 Toulouse, France

c GFZ German Research Centre for Geosciences, Potsdam, Germany

d Department of Earth Sciences, UCL, Gower Street, WC1E 6BT London, United Kingdom

ABSTRACT

The accurate interpretation of Si isotope signatures in natural systems requires knowledge of the equilibrium isotope fractionation between Si bearing solids and the dominant Si-bearing aqueous species. Aqueous silicon speciation is dominated by silicic acid ($H_4SiO_4^o$) in most natural aqueous fluids at pH <8.5, but forms $H_3SiO_4^-$, $H_2SiO_4^{2-}$, and polymeric Si species in more alkaline fluids. In this study isotope exchange experiments were performed at *bulk chemical* equilibrium between amorphous silica ($SiO_2 \cdot 0.32\ H_2O$) and inorganic aqueous fluids at pH ranging from 5.8 to 9.9 at 25° and 75°C with experiments running as long as 375 days. The 'three-isotope method' was used to quantify the equilibrium Si isotope fractionation, $\Delta_{eq}^{30}Si$, between amorphous silica and aqueous Si; at pH ~ 6 this equilibrium fractionation factor was found to be 0.45 ± 0.2 ‰ at 25ºC, and 0.07 ± 0.06 ‰ at 75°C. At more basic pH (> 9), equilibrium Si isotope fractionation factors between solid and aqueous solution are higher, at 1.63 ± 0.23 ‰ at 25ºC, and 1.06 ± 0.13 ‰ at 75°C. Taking account of the distribution of the aqueous Si species, equilibrium Si isotope fractionation factors between $H_3SiO_4^-$ and $H_4SiO_4^o$ of -2.34 ± 0.13 ‰ and -2.21± 0.05 ‰ at 25 and 75°C, respectively, were determined. The distinct equilibrium isotope fractionation factors of $H_3SiO_4^-$ and $H_4SiO_4^o$, and its variation with temperature can be used to establish paleo-pH and temperature proxies. The application of the three-isotope method also provides insight into the rates of isotopic exchange. For the solid grain size used (~20 nm), these rates match closely the measured bulk dissolution rates for amorphous silica for most of the isotope exchange process, suggesting the dominant and rate controlling isotope exchange mechanism in the experiments is detachment and reattachment of material at the amorphous silica surface.

1. INTRODUCTION

Silicon stable isotopes have been used as a tracer of a number of Earth (near-) surface processes, including weathering, biological activity, and marine paleo-temperature (e.g. De La Rocha et al., 1998; Ding et al., 2005; Ziegler et al., 2005a; Opfergelt et al., 2006, 2010, 2012, 2017; Georg et al., 2007; De La Rocha et al., 2011; Demarest et al., 2009; Hendry et al., 2011; Hendry and Robinson, 2012; Pogge von Strandmann et al., 2012; Pokrovsky et al., 2013; Marin-Carbonne et al., 2014; Oelze et al., 2014; Frings et al., 2015; He et al., 2016). The Si isotopic composition of many terrestrial reservoirs have been measured, including that of oceans, lakes, rivers and groundwaters (e.g. De La Rocha et al., 2000, 2011; Wischmeyer et al., 2003; Reynolds et al., 2006; Georg et al., 2009; Ding et al., 2011; Grasse et al., 2013; Pokrovsky et al., 2013; Frings et al., 2015), soils (Riotte et al., 2018a), plants (Douthitt, 1982; Ding et al., 2008a, 2008b; Pogge von Strandmann et al., 2012; Opfergelt et al., 2012; Riotte et al., 2018b), minerals, sedimentary rocks, cherts, and banded iron formations (e.g. Douthitt, 1982; Ziegler et al., 2005a, 2005b; Georg et al., 2009; Steinhoefel et al., 2010; van den Boorn et al., 2010; Savage et al., 2013). Constraining isotopic fractionation among these reservoirs is crucial to understanding the Si geochemical cycle.

Experimental studies have demonstrated that the Si isotopic signatures in natural environments can evolve during mineral precipitation (Li et al., 1995; Basile-Doelsch et al., 2005; Geilert et al., 2014, 2015; Roerdink et al., 2015; Oelze et al., 2015), mineral dissolution (Delvigne et al., 2012) or during adsorption of aqueous species (Delstanche et al., 2009; Oelze et al., 2014). Silicon isotopic fractionation during such mineral-aqueous fluid reactions in nature have been considered to be influenced by kinetic isotope fractionation (Geilert et al., 2014; Oelze et al., 2015; Roerdink et al., 2015; Poitrasson, 2017). However the degree of Si isotope fractionation at equilibrium is scarcely known, so that the relative impact of kinetic versus equilibrium processes on Si isotope fractionation during fluid-mineral interactions cannot be assessed unambiguously.

A critical factor to determine the equilibrium fractionation between a mineral and its coexisting aqueous fluid is the aqueous speciation of the system. The impact of aqueous speciation on the mineral/fluid fractionation factor has been demonstrated for elements such as boron, carbon, magnesium, mercury, transition metals and silicon (Hemming and Hanson, 1992; Zhang et al., 1995; Zeebe, 2005; Klochko et al., 2006, 2009; Asael et al., 2009; Holloway et al., 2011; Jiskra et al., 2012; Ryan et al., 2013; Yin et al., 2013; Fujii et al., 2014, 2015; Dupuis et al., 2015; Noireaux et al., 2015; Schott et al., 2016; Balan et al., 2018; Mavromatis

et al., 2019). Aqueous Si speciation depends on the solution pH and total dissolved Si concentration. In inorganic systems at ambient temperature, pH < 8.5 and $m_{Si} \leq 10^{-2.7}$ M (~ amorphous silica solubility), silicic acid ($H_4SiO_4^o$) dominates Si aqueous speciation. As pH increases, the species, $H_3SiO_4^-$ and $H_2SiO_4^{2-}$, form at the expense of silicic acid, whereas polymeric Si species become increasingly important in aqueous solutions supersaturated with respect to amorphous silica (Dietzel, 2000). At 75 °C, $H_4SiO_4^o$ will dominate only up to pH 7.8, where the species $H_3SiO_4^-$ starts form at the expense of aqueous silicic acid. Figure 1 shows the speciation of Si in an aqueous solution containing 1.6×10^{-3} M Si (corresponding to the equilibrium with amorphous silica at pH<9) as a function of pH for 25°C and 75°C, respectively. As the speciation of aqueous silicon changes with pH, equilibrium Si isotope fraction between this fluid and any Si bearing mineral will change accordingly (Dupuis et al., 2015; Fujii et al., 2015).

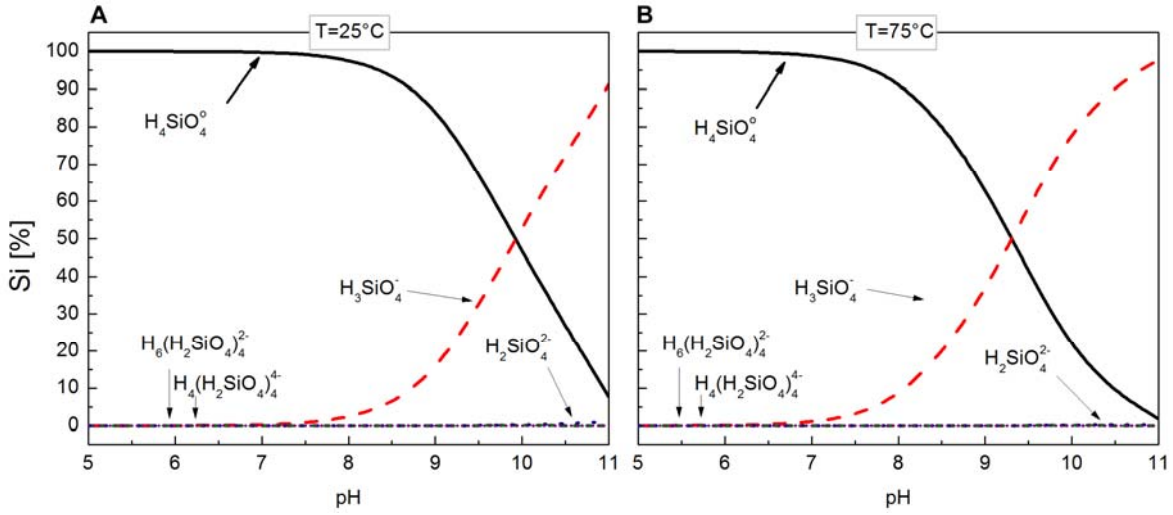

Fig. 1. Distribution of aqueous Si species in equilibrium with amorphous silica as a function of pH calculated with PHREEQC using its llnl database, for A. 25°C and B. 75°C. Notice that at 75°C the increase in the concentration of the $H_3SiO_4^-$ species occurs at a lower pH than at 25°C.

Several past studies attempted to determine Si fractionation factors between amorphous silica and its coexisting aqueous solutions (Geilert et al., 2014; Oelze et al., 2014; Roerdink et al., 2015). Most report an enrichment of the solid in light (^{28}Si) isotopes, which could be explained by non-equilibrium fractionation during precipitation of amorphous silica from a supersaturated solution (Dupuis et al., 2015). Zheng et al. (2016) measured Si isotopic fractionation at chemical equilibrium between a Fe(III)-bearing silica gel and artificial Archean seawater; they reported a 25°C equilibrium fractionation factor, $\Delta_{eq}{}^{30}Si_{gel\text{-}fluid}$ of ~ -3.5 ‰. Dupuis et al. (2015) used first-principle methods to calculate the 25 °C equilibrium fractionation factors between quartz and its co-existing aqueous solution, and kaolinite and its co-existing aqueous solution. These calculations predict a $\Delta_{eq}{}^{30}Si_{\ mineral\text{-}fluid}$ at neutral pH of 2.1 ± 0.2‰ and

0.4 ± 0.2‰, for the quartz-aqueous solution and kaolinite-aqueous solution system, respectively. Additionally these authors reported the 25°C equilibrium Si isotope fractionation factor, $\Delta_{eq}{}^{30}Si_{H_3SiO_4^- - H_4SiO_4^0}$= -1.6 ± 0.3‰, between the $H_3SiO_4^-$ and $H_4SiO_4^0$ aqueous silicon species. Similarly, Fujii et al. (2015) experimentally and theoretically determined the equilibrium fractionation factor between the two aqueous species $H_3SiO_4^-$ and $H_4SiO_4^0$. Their determined values of $\Delta_{eq}{}^{30}Si_{H_3SiO_4^- - H_4SiO_4^0}$= -3.5 ‰ (experimental) and $\Delta_{eq}{}^{30}Si_{H_3SiO_4^- - H_4SiO_4^0}$= -3 ‰ (ab initio calculations) are somewhat inconsistent with those calculated by Dupuis et al. (2015). These inconsistencies between the ab initio results of Fujii et al. (2015) and Dupuis et al. (2015) stem from the models used for the configuration of the Si aqueous species in solution. Fujii et al. (2015) assumed the aqueous Si consisted of static isolated clusters, whereas Dupuis et al. (2015) took into account the interactions of these clusters with surrounding water molecules as well as the configurational disorder of the solution.

The aim of this study is to expand on these past efforts, by determining experimentally the equilibrium fractionation factors between amorphous SiO_2 and the aqueous Si species $H_3SiO_4^-$ and $H_4SiO_4^0$ as a function of pH over a range of 5.8<pH<10 at temperatures of 25°C and 75°C. Experiments were performed at pH ~6, as silicic acid $H_4SiO_4^0$ will be the only silica species present in solution, and at pH ~9 where, in addition to $H_4SiO_4^0$, sufficient $H_3SiO_4^-$ is present but the presence of $H_2SiO_4^{2-}$ and potentially forming Si-O polymer species are insignificant. Results at these conditions will, therefore, allow the unambiguous determination of distinct equilibrium fractionation factors among amorphous SiO_2 and aqueous $H_3SiO_4^-$ and $H_4SiO_4^0$. To assure the attainment of isotopic equilibrium, the 'three-isotope method' was applied. The purpose of this paper is to report the results of this experimental study and provide new insights into how aqueous solution speciation and temperature can affect the Si equilibrium isotopic fractionation between amorphous silica and an aqueous solution.

2. THEORETICAL BACKGROUND

2.1 Geochemical calculations of amorphous silica dissolution rates

All geochemical calculations in this study were performed using PHREEQC (Parkhurst and Appelo, 2013) together with its llnl thermodynamic database. The standard state adopted in this study calls for unit activity of pure minerals, solids, and H_2O. For aqueous species, the standard state is unit activity of a 1 molal solution extrapolated to infinite dilution. The activity coefficients of charged aqueous species were calculated using the Davies equation, whereas the activity coefficients of neutral species were assumed to be equal to one.

The experiments in the present study were begun by first equilibrating an initially Si free aqueous solution of known pH with amorphous silica. The dissolution reaction for amorphous silica is described by:

$$SiO_{2,am} + 2\,H_2O \rightarrow H_4SiO_4^0 \quad (1)$$

The law of mass action for reaction (1) is given by

$$K_{eq} = \frac{a_{H_4SiO_4^0}}{a_{SiO_{2,am}} a_{H2O}^2} \quad (2)$$

where K_{eq} stands for an equilibrium constant and a_i refers to the activity of the subscripted species or phase. Taking account of this standard state, in pure water ($a_{H_4SiO_4^0} = C_{H_4SiO_4^0}$where C_i stands for the concentration of the subscripted species), Eqn. (2) reduces to

$$K_{eq} = C_{H_4SiO_4^0,eq} \quad (3)$$

where $C_{H_4SiO_4^0,eq}$ stands for the concentration of $H_4SiO_4^0$ in equilibrium with amorphous silica. The surface area normalised rates of amorphous silica dissolution (r) in a closed system and in the absence of specific inhibitors or catalysts can be described using (Rimstidt and Barnes, 1980)

$$r = \frac{dC_{H_4SiO_4^0}}{dt} = S/M\left(k_+ - k_- C_{H_4SiO_4^0}\right) \quad (4)$$

where S and M refer to the interfacial surface area and mass of aqueous solution in the reactor and k_+ and k_- designates amorphous silica dissolution and precipitation rate constants, respectively. Note $C_{H_4SiO_4^0}$ in Eqn. (4) has units of mol/kg H_2O. Rearranging Eqn. (4) and integrating it between times t= 0 and t gives

$$t = (1/k'_-) ln\left(\frac{k'_+ - k'_-.C_{H_4SiO_4^0}}{k'_+ - k'_-.C_{(H_4SiO_4^0)_0}}\right) \quad (5)$$

where $k'_+ = (\frac{S}{M})k_+$ and $k'_- = (\frac{S}{M})k_-$, and $C_{(H_4SiO_4^0)_0}$ denotes $C_{H_4SiO_4^0}$ at time zero. When starting from a zero concentration of $H_4SiO_4^0$ in solution, Eqn. (5) reduces to

$$t = (1/k'_-) ln\left(\frac{k'_+ - k'_-.C_{H_4SiO_4^0}}{k'_+}\right). \quad (6)$$

Noting that $\frac{k'_+}{k'_-} = C_{(H_4SiO_4^0)_{eq}}$, where $C_{(H_4SiO_4^0)_{eq}}$ again denotes the concentration of dissolved silica in equilibrium with amorphous silica, the temporal evolution of dissolved silica concentration in the closed system is described by

$$C_{H_4SiO_4^0} = C_{(H_4SiO_4^0)_{eq}}\left(1 - e^{-t.k'_-}\right) \quad (7)$$

2.2. Si isotope systematics

Silicon isotope compositions in this study are reported using the standard δ-notation in per mil (‰) relative to the international NBS-28 standard (NIST RM-8546), computed using:

$$\delta^{x}\mathrm{Si} = \left[\frac{(^{x}\mathrm{Si}/^{28}\mathrm{Si})_{Sample}}{(^{x}\mathrm{Si}/^{28}\mathrm{Si})_{NBS-28}} - 1\right] \quad (8)$$

Where $(^{x}\mathrm{Si}/^{28}\mathrm{Si})_{sample}$ refers to the atomic ratio of the Si with mass *x,* which denotes either ^{29}Si or ^{30}Si, to that of ^{28}Si in the sample of interest. The Si isotopic fractionation factor between a solid and an aqueous fluid ($\alpha^{x/28}_{solid-fluid}$) is defined as:

$$\alpha^{x/28}_{solid-fluid} = \frac{(^{x}\mathrm{Si}/^{28}\mathrm{Si})_{solid}}{(^{x}\mathrm{Si}/^{28}\mathrm{Si})_{fluid}} \quad (9)$$

The silicon isotopic fractionation between a solid and a coexisting aqueous phase can be also described using $\Delta^{x}\mathrm{Si}_{solid-fluid}$, which is defined by

$$\Delta^{x}\mathrm{Si}_{solid-fluid} = \delta^{x}\mathrm{Si}_{solid} - \delta^{x}\mathrm{Si}_{fluid} \quad (10)$$

Note that $\Delta^{x}\mathrm{Si}_{solid-fluid}$ is approximately related to $\alpha^{x/28}_{solid-fluid}$ by

$$\Delta^{x}\mathrm{Si}_{solid-fluid} \approx 10^{3} ln\alpha^{x/28}_{solid-fluid} . \quad (11)$$

The fractionation factor between the solid and the aqueous fluid depends on the proportion of the different species, *i*, present in this fluid and their individual fractionation factors with the solid, $\alpha^{x/28}_{solid-i}$, consistent with (Zhang et al., 1995):

$$10^{3} ln\alpha^{x/28}_{solid-fluid} = \sum_{i}(x_i \times 10^{3} ln\alpha^{x/28}_{solid-i}) \quad (12)$$

where x_i refers to the mole fraction of the dissolved Si present in the *ith* aqueous species.

2.3. Three-isotope method

Equilibrium fractionation factors in the present study were generated using the three-isotope method. The three-isotope method was originally used to determine the equilibrium isotopic fractionation factors of oxygen between mineral and co-existing aqueous solutions (Matsuhisa et al., 1978; Matthews et al., 1983a, 1983b, 1983c). Over the past 10 years, this method was also successfully applied to non-traditional isotopic systems, such as Mg and Fe (Shahar et al., 2008; Beard et al., 2010; Li et al., 2011; Frierdich et al., 2014; Reddy et al., 2015), as well as to Si (Zheng et al., 2016). This approach has also been used to evaluate the kinetics of isotopic exchange reactions between two components (Cole and Chakraborty, 2001; Johnson et al., 2002; Li et al., 2011; Wu et al., 2012; Zheng et al., 2016). Before exchange, one component (Phase A, typically the solid) exhibits a "natural" isotopic composition and plots on a δ vs. δ diagram, such as Fig. 2, on a primary fractionation line, also known as the terrestrial

fractionation line (TFL). This line follows a mass-dependent relation where $\delta^{30}Si \approx 1.93 \times \delta^{29}Si$ (Young et al., 2002). The second component (Phase B, typically the fluid) is enriched in one isotope (for example, ^{29}Si in the present study) and thus has a distinct and known offset from the TFL. As the system undergoes isotopic exchange, the isotopic compositions of the two components will gradually evolve over time (*t*) towards isotopic equilibrium. Once the isotopic exchange is complete and isotopic equilibrium has been attained, the isotopic compositions of the two phases will fall on a secondary fractionation line (SFL) parallel to the TFL. The position of the SFL can be determined from the isotopic mass balance of the system (see Fig. 2).

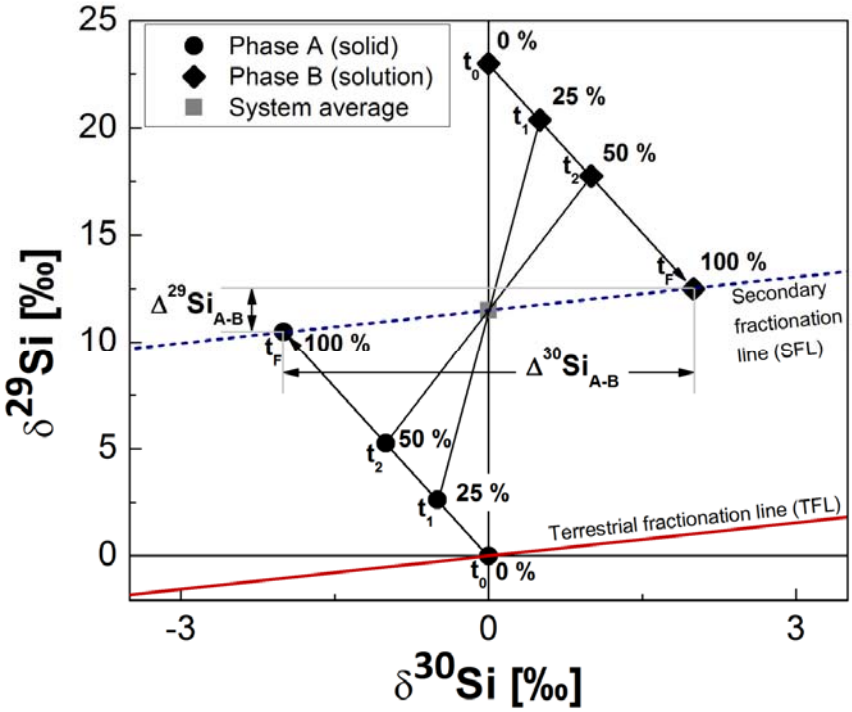

Fig. 2. Schematic diagram of the three-isotope method applied to Si, modified after Li et al. (2011) and Zheng et al. (2016). At time (t) zero, and in the absence of isotopic exchange (shown in %), Phase A plots as the isotopically "normal" component on the terrestrial fractionation line (TFL). At t0 Phase B shows a distinct offset from the TFL as it is enriched in 29Si. The isotopic composition of phases A and B gradually evolve towards 100% isotopic exchange. The lines connecting the two phases at a given time always cross the system average as required by isotope mass balance. When isotopic exchange is complete, the two phases plot on a secondary fractionation line, whose position is dictated by the isotopic mass balance of the system.

For many systems, isotopic exchange is slow and therefore often incomplete. The three-isotope method, nevertheless, allows for the determination of *equilibrium fractionation factors* through the determination of the degree of isotope exchange (*F*). The degree of isotopic exchange is defined by

$$F = \frac{(\delta_t - \delta_i)}{(\delta_e - \delta_i)} \quad (13)$$

where δ_t denotes the isotopic composition of either one of the phases at any time, t, during the isotope exchange reaction, and δ_i and δ_e describe the initial and equilibrium isotopic composition of this phase. The parameter F ranges from 0 to 1 as isotopic equilibrium is attained. In a two-component system δ_e can be derived from the mass balance constraints (Zheng et al., 2016), and calculated from

$$\delta_e = \delta_{mean} - \left(\frac{N_{solid}}{N_{solid}+N_{fluid}}\right) \times \Delta_{eq,solid-fluid} \quad (14)$$

where δ_{mean} in this study stands for the mass averaged Si isotope composition of the system, $\Delta_{eq,solid\text{-}fluid}$ designates the *equilibrium isotope fractionation factor* between the solid and fluid phases, and N_{solid} and N_{fluid} denote the number of moles of Si in the solid and fluid phase, respectively. If the $\Delta_{eq,solid\text{-}fluid}$ of the system is not known, as is the case in the present study, it can be obtained from an iterative fit of experimental data (Zheng et al., 2016).

2.4. Kinetics of isotopic exchange

The 'three-isotope method' not only allows determination of the equilibrium fractionation factors of a solid-fluid system, but also allows determination of the kinetics of isotopic exchange. Following the approach of Cole and Chakraborty (2001) and Johnson et al. (2002) isotope exchange rates can be quantified using

$$\frac{-d(1-F)}{dt} = k_n(1-F)^n \quad (15)$$

where k_n stands for the rate constant of reaction order n, this reaction order is usually an integer from 0 to 3. Isotope exchange reactions typically follow either a first-order (n=1) or second-order (n=2) rate law (Criss et al., 1987; Huang and Tsai, 1970; Johnson et al., 2002; Welch et al., 2003; Li et al., 2011; Zheng et al., 2016). The integrated form of this rate equation can be written as either

$$\ln(1-F) = -k_1 t \quad (16)$$

for n=1

$$\frac{F}{(1-F)} = k_2 t \quad (17)$$

for n=2.

Isotope exchange rate constants can be quantified by fitting the experimental value of F to Eqn. (16) for the first order rate constant or Eqn. (17) for the second order rate constant (Cole and Chakraborty, 2001; Johnson et al., 2002; Li et al., 2011).

3. METHODS

3.1. Experimental approach

3.1.1. Starting powder - amorphous silica

All experiments in the present study were performed in series using Alpha Aeser® 100 mesh hydrated silicic acid powder. This powder was cleaned prior to each experimental series by sedimentation in >18.2 Ω de-ionized water (Milli-Q®) to remove ultrafine particles (Pokrovski and Schott, 1998). In each case, from 40 to 75 g of the hydrated silicic acid powder was suspended by stirring in a 1dm^3 glass beaker. The powder was sedimented for 10 minutes and then decanted. This operation was repeated until the supernatant became clear within the first 5 min. Subsequently the powder was oven dried at 60°C. To avoid hydration of the powder it was placed into a desiccator while it cooled to room temperature. Representative scanning electron microscope (SEM) and transmission electron microscope (TEM) images of the resulting powders are shown in Fig. 3A and B.

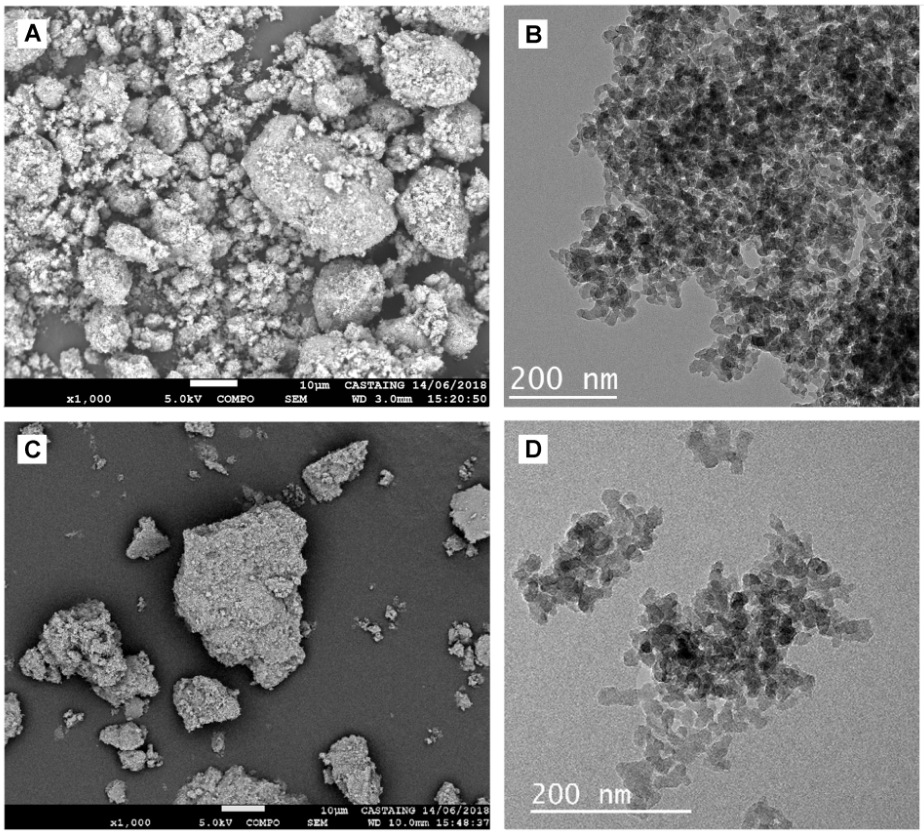

Fig. 3. Representative images of amorphous SiO2 powders. A) SEM image of the initial powder showing agglomerates of amorphous SiO2 grains. B) TEM image of the initial powder showing rounded ~ 21 nm SiO2 grains. C) Representative SEM image of reacted amorphous silica powder. D) TEM image of reacted amorphous silica recovered from the longest duration experiment performed at T ~25°C, pH ~6.

These images were acquired using a MEB JEOL JSM-7800F Prime electron microscope and a JEOL JEM-ARM200F Cold FEG transmission electron microscope at the Raimond Castaing Microcharacterization Centre (Toulouse, France), respectively. The TEM images were used to measure average grain size with the ImageJ software package (Schindelin et al., 2012); the average measured grain size of the cleaned dried amorphous silica was ~21 ± 5 nm (2SD, n=100). Energy dispersive spectroscopy (EDS) analyses indicate the prepared powder contained no metals other than Si. Thermogravimetric analyses, performed with a Mettler Toledo® ATG/DSC1, showed that the powders also contained ~8.7 % H_2O, which is consistent with the chemical formula $SiO_2 \cdot 0.32\ H_2O$. The specific surface areas of the cleaned amorphous silica were determined with a Quantachrome Autosorb-1MP using the nitrogen multipoint BET method (Brunauer et al., 1938). The average surface area of the initial amorphous silica powders is 196.3 m^2/g, and ranged from 175 m^2/g to 215 m^2/g with an estimated uncertainty of ± 10%.

3.1.2. Initial aqueous solutions

The initial aqueous solutions used in the experiments were prepared using high purity de-ionized Milli-Q® water (>18.2 Ω), and reagent grade HCl, NH_4OH and NH_4Cl; the compositions of these initial solutions are provided in Table 1. These solutions had a pH of ~6 and ~10 for the 25°C experiments and ~6 and ~9 for the 75°C experiments; experiments run with these fluids are labelled SibA, SicB, SigA, and SikB, respectively. The pH of these fluids were selected as at pH < 8.5 for 25°C and pH < 7.8 at 75°C, aqueous silicic acid ($H_4SiO_4^o$) will be the only significant silica species present in solution. At pH 9.9 at 25°C and 9.1 at 75°C, aqueous $H_3SiO_4^-$ will have formed at the expense of aqueous silicic acid and both will have a similar species distribution of ~50% $H_4SiO_4^o$ and ~50% $H_3SiO_4^-$. This enables quantification of the effect of the aqueous $H_3SiO_4^-$ species on equilibrium fractionation factors at these two temperatures.

3.1.3. Characterization of the aqueous solutions

The aqueous solution pH was regularly monitored during the experiments with a Metrohm® 913 pH Meter connected to a standard glass microelectrode. This electrode was calibrated using certified Orion Thermo Scientific® buffers. The uncertainty in the measurements was determined to be 0.05, equal to 2 standard deviations of ~40 repeated measurements of the pH=4.01 calibration standard. For experiments at 75°C, the pH was measured at 25°C and later calculated to this higher temperature with PHREEQC.

Aqueous silicon concentrations were determined by the molybdate blue method (Truesdale and LeCorre, 1975) using a Bran & Luebbe® analyser-III colorimeter coupled to a Seal XY-2 autosampler and a Technicon analyser II mixing unit. The measurements were conducted over the 0.1 to 10 ppm concentration range. The long-term reproducibility of these measurements was determined to be within 3% and the quantification limit was 0.04 ppm. To verify that aqueous Si polymerisation did not occur in the reactive fluids during the experiments, additional Si concentration measurements were performed on selected fluid samples by ICP-OES. In all cases the aqueous Si concentrations measured by ICP-OES were equal to within uncertainty of corresponding values measured by colorimetry confirming that silica polymerisation was negligible.

3.1.4. Experiment design: Step 1 Equilibration of reactive fluids

Experiments in this study were conducted in four distinct series. Each series began by equilibrating 200 ml of an initial aqueous fluid with 3 g of pre-washed amorphous SiO_2 powder in closed polypropylene bottles (see Table 1). Once closed, these bottles were placed in shaking thermostatic baths at either ~25°C or ~75°C. The aqueous fluids in the bottles were sampled 8 times at regular intervals during the 19 to 65 days of this equilibration step. The pH was measured immediately after each sampling at room temperature. The samples collected from the 75°C experiments were then diluted to prevent precipitation. Aqueous Si concentrations were determined by colorimetry on all samples and by ICP-OES on selected samples. Chemical equilibrium was assumed to be reached when both pH and the Si concentration of the aqueous solutions attained constant values within uncertainty. This initial step was stopped once these constant values were reached. The fluids were then filtered with Merck® 0.2 µm Teflon syringe filters. Fluids recovered from the 75°C experiments were kept in the thermostatic bath until subsequently used in the isotopic exchange experiments described below.

Table 1. Summary of the initial conditions of the first step of each experimental series performed in the present study. Quantity in grams of fluids and solids used are denoted as $m_{initial\ sol}$ and $m_{SiO_2,am.}$

Experiment ID	Temperature [°C]	Initial aqueous solution composition	pH	$m_{initial\ sol}$ [g]	$m_{SiO_2,am}$ [g]
SibA	25	pure MQ® water + 0.43 ml 1 N HCl + 0.50 ml 1.4 N NH_4OH	6.2	200.04	3.00
SicB	25	0.1 M NH_4Cl - 0.35 M NH_4OH	10.2	200.00	3.00
Sig75A	75	pure MQ® water	6.0	200.21	3.02
Sik75B	75	0.1 M NH_4Cl - 1.52 M NH_4OH	9.4	200.56	3.01

3.1.5. Experiment design: Step 2 Isotopic exchange experiments

The four chemical equilibrated fluids were enriched with a ^{29}Si isotope tracer to obtain a $\delta^{29}Si = \sim 23‰$ (see Table 2). The added ^{29}Si isotope tracer was prepared by dissolving Eursio-top® $^{29}SiO_2$ powder, having an initial composition of 0.21% ^{28}Si, 99.76% ^{29}Si, and 0.03% ^{30}Si in de-ionized water. After the addition of this spike to the equilibrated fluids, the Si concentration and pH were measured. The fluid pH was adjusted, if necessary, by adding a small quantity of HCl or NH_4OH to assure these initial fluids were as close to equilibrium with amorphous silica as possible. Each series of isotopic exchange experiments consisted of a suite of 8 closed system experiments of the selected durations listed in Table 2. This approach was selected so that both the solids and fluids could be collected and analysed after these distinct experiment durations. The overall duration of each experimental series were selected so that degree of isotopic exchange would approach 1 at the end of each series. Each individual experiment was performed in 10 ml polypropylene reactors. Into each reactor was added ~ 0.15 g of amorphous SiO_2 powder with a known Si isotope composition and 5 ml of the prepared ^{29}Si enriched fluid. The 25°C experiments were placed into an orbital shaker to be constantly mixed. The 75°C experiments were placed into a thermostatic bath and hand shaken once or twice a day. To verify that no leakage occurred during any experiment, all reactors were weighted both at the beginning and the end of each experiment. At pre-chosen time intervals, a reactor was centrifuged for 20 min at 4500 rpm and then opened. The supernatant was separated from the powder and filtered using Merck® 0.2 µm Teflon syringe filters. The pH was measured immediately after sampling, and fluids recovered from the 75°C experiments were diluted just after measuring pH. The recovered powder was gently rinsed with de-ionized water on a 0.2 µm filter, oven-dried at 40°C, and stored for further analysis. It is unlikely that this rinsing altered significantly the isotopic composition of the recovered solid due to the low solubility and dissolution kinetics of the solid.

Table 2. Overview of the results of the isotopic exchange experiments performed in this study. Uncertainties of the isotopic measurements are expressed as 2 SD (Standard Deviation), and 2 SE (Standard Error). The 2 SE is computed following the relation: $SE = \frac{SD}{\sqrt{(n-1)}} \times t$, where n denotes the number of measurements performed, and t denotes the Student t-factor (Platzner et al., 1997). δ_{eq} represents the equilibrium isotopic composition of ^{29}Si and F denotes the degree of isotopic exchange. [a] denotes the spiked initial solution.

Exp. ID	Elapsed Time	Temp.	pH	Si-conc.	S_{BET}	*Aqueous solution*						*amorphous SiO_2*						$\delta_{eq}{}^{29}Si$	*F*	ln(1-*F*)
	[d]	[°C]		[ppm]	[m^2/g]	$\delta^{30}Si$	2SD	2SE	$\delta^{29}Si$	2SD	2SE	$\delta^{30}Si$	2SD	2SE	$\delta^{29}Si$	2SD	2SE			
						[‰]	[‰]	[‰]	[‰]	[‰]	[‰]	[‰]	[‰]	[‰]	[‰]	[‰]	[‰]	[‰]		
SibA:																		-0.22		
SibA 0	0	25	6.2	44.40	214.7	***-0.69***	*0.20*	*0.10*	***-0.33***	*0.10*	*0.05*	***-0.07***	*0.18*	*0.11*	***-0.06***	*0.03*	*0.02*			
SibA – S[a]	0	25	6.1	47.96		***-0.63***	*0.13*	*0.07*	***22.85***	*0.16*	*0.08*	***-0.07***	*0.18*	*0.11*	***-0.06***	*0.03*	*0.02*		0.000	0.00
SibA 1	0.25	25	6.4	47.40		***-0.55***	*0.15*	*0.12*	***14.23***	*0.16*	*0.13*	***0.00***	*0.15*	*0.12*	***0.03***	*0.09*	*0.07*		0.374	-0.47
SibA 2	1	25	6.5	48.16		***-0.47***	*0.20*	*0.16*	***10.14***	*0.05*	*0.04*	***-0.07***	*0.10*	*0.08*	***0.01***	*0.03*	*0.03*		0.551	-0.80
SibA 3	3	25	6.3	48.48		***-0.55***	*0.09*	*0.11*	***6.16***	*0.06*	*0.07*	***-0.01***	*0.20*	*0.16*	***0.05***	*0.03*	*0.02*		0.723	-1.29
SibA 4	10	25	6.4	49.11		***-0.54***	*0.08*	*0.10*	***3.74***	*0.17*	*0.21*	***-0.01***	*0.12*	*0.10*	***0.05***	*0.12*	*0.10*		0.828	-1.76
SibA 5	30	25	6.5	49.78		***-0.82***	*0.12*	*0.14*	***2.42***	*0.08*	*0.10*	***-0.09***	*0.10*	*0.13*	***0.03***	*0.07*	*0.09*		0.886	-2.17
SibA 6	66	25	6.4	50.06		***-0.77***	*0.11*	*0.13*	***1.88***	*0.02*	*0.02*	***-0.13***	*0.04*	*0.05*	***0.04***	*0.10*	*0.12*		0.909	-2.39
SibA 7	171	25	6.4	56.99		***-0.61***	*0.05*	*0.06*	***1.33***	*0.08*	*0.10*	***-0.08***	*0.09*	*0.12*	***0.02***	*0.03*	*0.03*		0.933	-2.70
SibA 8	351	25	6.4	53.84	137.1	***-0.29***	*0.17*	*0.09*	***0.14***	*0.17*	*0.09*	***-0.08***	*0.10*	*0.13*	***0.04***	*0.03*	*0.04*		0.984	-4.17
SicB:																		-0.54		
SicB 0	0	25	10.1	116.24	195.0	***-1.62***	*0.09*	*0.06*	***-0.84***	*0.05*	*0.03*	***-0.09***	*0.12*	*0.15*	***-0.03***	*0.03*	*0.04*			
SicB 0-S[a]	0	25	9.9	115.42		***-1.57***	*0.07*	*0.04*	***23.30***	*0.19*	*0.10*	***-0.09***	*0.12*	*0.15*	***-0.03***	*0.03*	*0.04*		0.000	0.00
SicB 1	0.25	25	9.8	114.73		***-1.24***	*0.04*	*0.03*	***3.04***	*0.02*	*0.01*	***-0.06***	*0.05*	*0.06*	***0.16***	*0.02*	*0.03*		0.850	-1.90
SicB 2	1	25	9.9	115.58		***-1.34***	*0.17*	*0.14*	***2.00***	*0.09*	*0.07*	***-0.09***	*0.02*	*0.02*	***0.14***	*0.00*	*0.01*		0.893	-2.24
SicB 3	3	25	9.9	120.73		***-1.43***	*0.17*	*0.22*	***1.81***	*0.08*	*0.09*	***-0.12***	*0.09*	*0.11*	***0.18***	*0.05*	*0.06*		0.901	-2.31
SicB 4	10	25	9.9	119.87		***-1.56***	*0.14*	*0.18*	***1.15***	*0.05*	*0.06*	***-0.09***	*0.10*	*0.13*	***0.21***	*0.03*	*0.03*		0.929	-2.64
SicB 5	30	25	9.9	115.31		***-1.65***	*0.16*	*0.20*	***0.42***	*0.21*	*0.27*	***-0.09***	*0.06*	*0.07*	***0.17***	*0.06*	*0.08*		0.960	-3.21
SicB 6	66	25	9.8	110.97		***-1.77***	*0.03*	*0.04*	***0.27***	*0.07*	*0.08*	***-0.10***	*0.07*	*0.09*	***0.21***	*0.02*	*0.02*		0.966	-3.38
SicB 7	179	25	9.9	106.02		***-1.62***	*0.20*	*0.16*	***0.02***	*0.11*	*0.09*	***-0.09***	*0.05*	*0.07*	***0.18***	*0.02*	*0.03*		0.976	-3.75
SicB 8	385	25	9.6	104.27	164.1	***-1.69***	*0.20*	*0.16*	***0.00***	*0.08*	*0.06*	***-0.05***	*0.04*	*0.04*	***0.24***	*0.12*	*0.15*		0.977	-3.79

Exp. ID	Elapsed Time	Temp.	pH	Si-conc.	S_{BET}	*Aqueous solution*						*amorphous SiO_2*						$\delta_{eq}{}^{29}Si$	*F*	ln(1-*F*)
	[d]	[°C]		[ppm]	[m^2/g]	$\delta^{30}Si$	2SD	2SE	$\delta^{29}Si$	2SD	2SE	$\delta^{30}Si$	2SD	2SE	$\delta^{29}Si$	2SD	2SE			
						[‰]	[‰]	[‰]	**[‰]**	[‰]	[‰]	**[‰]**	[‰]	[‰]	**[‰]**	[‰]	[‰]	[‰]		
Sig75A																		0.11		
Sig75A 0	0	75	5.8	117.36	195.6	***-0.02***	*0.15*	*0.12*	***0.00***	*0.09*	*0.07*	***-0.04***	*0.14*	*0.17*	***-0.03***	*0.13*	*0.17*			
Sig75A S[a]	0	75	5.2	122.27		***-0.10***	*0.25*	*0.16*	***22.87***	*0.09*	*0.06*	***-0.04***	*0.14*	*0.17*	***-0.03***	*0.13*	*0.17*		0.000	0.00
Sig75A 1	0.25	75	5.8	119.03		***-0.12***	*0.10*	*0.06*	***14.13***	*0.10*	*0.06*	***-0.08***	*0.17*	*0.10*	***0.09***	*0.11*	*0.07*		0.384	-0.48
Sig75A 2	1	75	5.8	115.55		***-0.23***	*0.09*	*0.07*	***8.54***	*0.01*	*0.01*	***-0.12***	*0.03*	*0.04*	***0.12***	*0.05*	*0.06*		0.629	-0.99
Sig75A 3	3	75	5.9	114.94		***-0.22***	*0.12*	*0.15*	***5.12***	*0.06*	*0.07*	***-0.08***	*0.05*	*0.06*	***0.18***	*0.01*	*0.02*		0.780	-1.51
Sig75A 4	10	75	6.2	113.90		***-0.18***	*0.16*	*0.10*	***3.72***	*0.09*	*0.06*	***-0.18***	*0.04*	*0.05*	***0.20***	*0.05*	*0.06*		0.841	-1.84
Sig75A 5	21	75	5.8	114.35		***-0.22***	*0.26*	*0.16*	***3.07***	*0.09*	*0.05*	***-0.14***	*0.02*	*0.02*	***0.18***	*0.07*	*0.09*		0.870	-2.04
Sig75A 6	33	75	5.8	118.59		***-0.22***	*0.28*	*0.17*	***2.65***	*0.05*	*0.03*	***-0.16***	*0.08*	*0.10*	***0.20***	*0.07*	*0.09*		0.888	-2.19
Sig75A 7	43	75	5.9	114.59		***-0.20***	*0.18*	*0.11*	***2.40***	*0.07*	*0.04*	***-0.09***	*0.11*	*0.07*	***0.22***	*0.06*	*0.04*		0.899	-2.30
Sig75A 8	55	75	6.0	109.54	171.7	***-0.13***	*0.14*	*0.11*	***2.09***	*0.07*	*0.06*	***-0.14***	*0.06*	*0.08*	***0.20***	*0.04*	*0.05*		0.913	-2.44
Sik75B																		0.01		
Sik75B 0	0	75	9.3	282.22	179.8	***-1.50***	*0.11*	*0.14*	***-0.76***	*0.08*	*0.10*	***-0.04***	*0.15*	*0.09*	***0.02***	*0.06*	*0.04*			
Sik75B S[a]	0	75	9.2	287.16		***-1.57***	*0.14*	*0.09*	***23.14***	*0.26*	*0.16*	***-0.04***	*0.15*	*0.09*	***0.02***	*0.06*	*0.04*		0.000	0.00
Sik75B 1	0.25	75	9.1	232.98		***-1.00***	*0.06*	*0.25*	***3.02***	*0.02*	*0.09*	***-0.12***	*0.07*	*0.06*	***0.45***	*0.07*	*0.05*		0.870	-2.04
Sik75B 2	1	75	9.1	237.19		***-1.10***	*0.13*	*0.10*	***1.60***	*0.11*	*0.09*	***0.01***	*0.22*	*0.14*	***0.50***	*0.16*	*0.10*		0.931	-2.67
Sik75B 3	3	75	9.1	227.35		***-1.18***	*0.11*	*0.08*	***1.17***	*0.08*	*0.06*	***-0.02***	*0.21*	*0.13*	***0.54***	*0.13*	*0.08*		0.950	-2.99
Sik75B 4	10	75	9.0	205.88		***-1.30***	*0.18*	*0.14*	***0.76***	*0.07*	*0.06*	***-0.06***	*0.17*	*0.10*	***0.53***	*0.06*	*0.04*		0.968	-3.43
Sik75B 5	21	75	8.9	178.02		***-1.27***	*0.14*	*0.18*	***0.71***	*0.07*	*0.08*	***0.05***	*0.20*	*0.25*	***0.57***	*0.04*	*0.06*		0.970	-3.50
Sik75B 6	33	75	8.7	163.55	119.0	***-1.18***	*0.15*	*0.18*	***0.64***	*0.12*	*0.15*	***-0.08***	*0.17*	*0.21*	***0.55***	*0.09*	*0.11*		0.973	-3.60
Sik75B 7	43	75	8.6	137.30		***-1.15***	*0.14*	*0.17*	***0.60***	*0.10*	*0.13*	***0.05***	*0.08*	*0.10*	***0.57***	*0.09*	*0.11*		0.974	-3.66
Sik75B 8	55	75	8.5	118.23		***-1.09***	*0.08*	*0.10*	***0.61***	*0.05*	*0.06*	***0.03***	*0.15*	*0.19*	***0.54***	*0.02*	*0.02*		0.974	-3.64

3.2. Si isotope analysis

Silicon isotope compositions were measured in the fluid and solid samples collected from all isotope exchange experiments, as well as the initial washed SiO_2 powders, the spiked initial fluid and the non-spiked chemical equilibrated fluids. Aqueous samples were prepared by first acidifying the solutions using bi-distilled 3N HCl to pH ~2. Amorphous silica powders were processed using the alkali fusion method described by Zambardi and Poitrasson (2011). From 2 to 5 mg of the solids were weighted into silver crucibles (XRF scientific, Montreal, Canada) together with a ~200 mg Merck® NaOH pellet. The crucibles were capped and placed into a furnace heated at 720°C for 10 min. They were subsequently cooled to room temperature and placed into 30 cm^3 Savillex® Teflon beakers filled with 20 ml Milli-Q® water for 24 hours to dissolve the fusion cake. The resulting fluids were then transferred to 60 cm^3 polypropylene bottles and diluted to 40 ml by adding Milli-Q® water. These 40 ml samples were then acidified using ~10 N bi-distilled HCl to obtain a pH of 1.5.

All prepared Si-bearing fluids generated from either the solid or fluid samples were purified by cation-exchange chromatography using the Bio-Rad® AG50W-12X cationic resin (Georg et al., 2006; Zambardi and Poitrasson, 2011). The detailed cleaning procedure of the resin is described in Zambardi and Poitrasson (2011). From 0.5 to 2 ml of prepared fluids containing up to 70 µg Si were loaded, directly collected, and eluted twice with Milli-Q® water to obtain 6 ml samples. These were then diluted and acidified to obtain a 3 ppm solution with a total 0.05 M HCl concentration. Silicon recovery after processing was determined to be between 90 to 100 %. The ^{28}Si signal of the procedural blank, processed in the same way, was found to be less than < 2% and was thus considered as negligible.

Silicon isotope ratios were determined using a Thermo Scientific Neptune® MC-ICP-MS either at the Observatoire Midi Pyrenées / Laboratorie Géosciences Environnement Toulouse (GET), France, or the GeoForschungsZentrum (GFZ) in Potsdam, Germany. Measurements were performed in medium resolution under either wet plasma at the GET or dry plasma conditions and the GFZ. Two different methods were used as these analyses were performed in different laboratories, which routinely use different procedures for Si isotope analyses. Measurements performed on several identical samples at these laboratories yielded identical results within uncertainty. The wet plasma samples were introduced with a Thermo SIS system with a double-pass cyclonic spray chamber. An ESI ApexHF desolvator (having sample path made of Perfluoroalkoxy alkane, PFA) and fitted with a PFA nebulizer was used for dry plasma conditions at the GFZ (Schuessler and von Blanckenburg, 2014). The

instrumental mass bias drift was corrected using the sample standard bracketing technique relative to NBS-28 (NIST SRM 8546), combined with Mg doping as an internal standard in all measured samples and standards. Measurements of $^{25}Mg/^{24}Mg$ ratios were performed in the dynamic mode, alternating between Si and Mg isotopes. Russell's exponential law (Russell et al., 1978) was then used to correct for the mass bias drift. The accuracy and precision of the isotopic analysis were validated by repeated measurement of the BHVO-2 reference material. They yielded a long-term reproducibility of $\delta^{30}Si$= -0.26 ± 0.13 ‰ for the GET analyses (2 S.D, n=59) and $\delta^{30}Si$= -0.28 ± 0.09 ‰ for the GFZ analyses (2 S.D, n=18), which are in close agreement with measurements reported in previous studies (e.g. Abraham et al., 2008; Zambardi and Poitrasson, 2011; Savage et al., 2013, 2014).

4. RESULTS

4.1 Attainment of fluid-amorphous SiO_2 equilibrium during the fluid equilibration step

Each experimental series began by equilibrating the initial Si-free fluids with the pre-treated amorphous SiO_2. The temporal evolution of dissolved Si concentration and pH in these fluids are provided in Table A of the electronic supplement; the Si concentrations are also shown in Fig. 4.

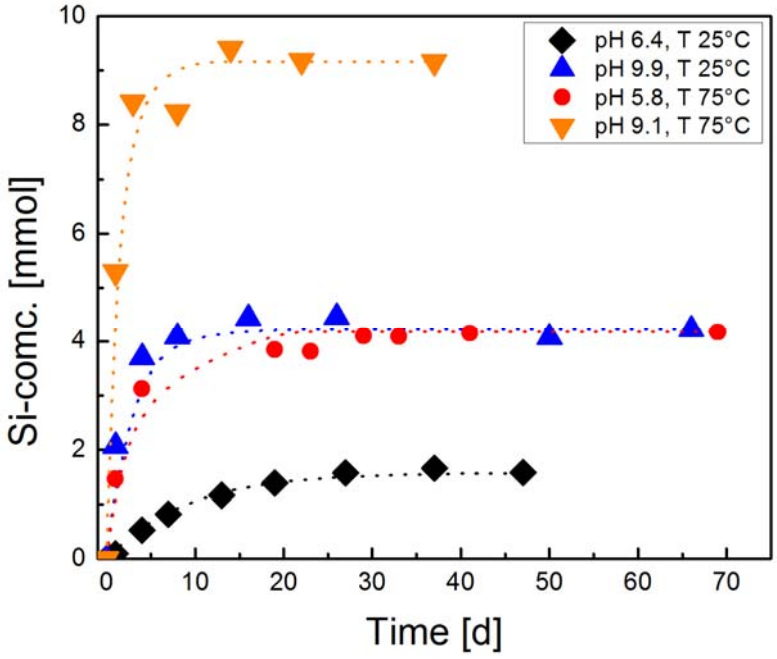

Fig. 4. Temporal evolution of dissolved Si concentration during the equilibration of the initial reactive fluids with amorphous silica during the first step of each experimental series. The dashed lines represent a fit of the data using Eqn. 7 with values of rate constant k'. listed in Table 3.

The Si concentration of the initial fluids at both 25° and 75° systematically increase to a constant maximum value. The constant final Si concentrations were within 10 % of those calculated to be in equilibrium with amorphous SiO_2 using PHREEQC. The curve drawn through these measured Si concentrations correspond to a fit of these data to Eqn. (7); the rate constants obtained by this regression are provided in Table 3.

Table 3. Concentration of aqueous Si in equilibrium with amorphous silica and dissolution rate constants and rates obtained from the first step of the four experimental series runs in this study.

Exp. Series	Si-conc.$_{equilibriun}$ [mmol]	k'_{-} [1/s]	k_{+} [mol/(m²*s)]
SibA	1.58	1.36×10^{-6}	3.13×10^{-12}
SicB	4.22	4.63×10^{-6}	2.85×10^{-11}
Sig75A	4.18	4.05×10^{-6}	2.47×10^{-11}
Sik75B	9.16	9.26×10^{-6}	1.24×10^{-10}

4.2 Results of Isotope exchange experiments

4.2.1. Observations on the solid phases

SEM and TEM images of amorphous SiO_2 collected from the longest duration experiment run of each experimental series were obtained; representative images are provided in Fig. 3 C and D. These images show that these final solids contain only amorphous SiO_2, and are identical in appearance to the pre-experiment, pre-treated solids.

A summary of the various measured characteristics of the solids collected after the longest duration experiment of each series is provided in Table B of the electronic supplement. The measured grain sizes of the collected final solids were 20 ± 1 nm (n=85, 2 S.D.), which are identical, within uncertainty, to the corresponding pre-treated solids. The water content of these final solids was measured at 8.4% by TGA, which is identical within uncertainty to that of the original pre-treated solids. Measured BET surface areas of the final reacted powders are somewhat lower than those of the original pre-treated solids; the largest decreases were those of the final pH 6.4, 25°C experiment and the final pH 9.1, 75°C experiment, which exhibited a decrease of ~35%. This could result from Ostwald ripening affecting the silica grains during the runs. Overall the post-experiment solids, however, appear to have been essentially unchanged by these isotope exchange experiments.

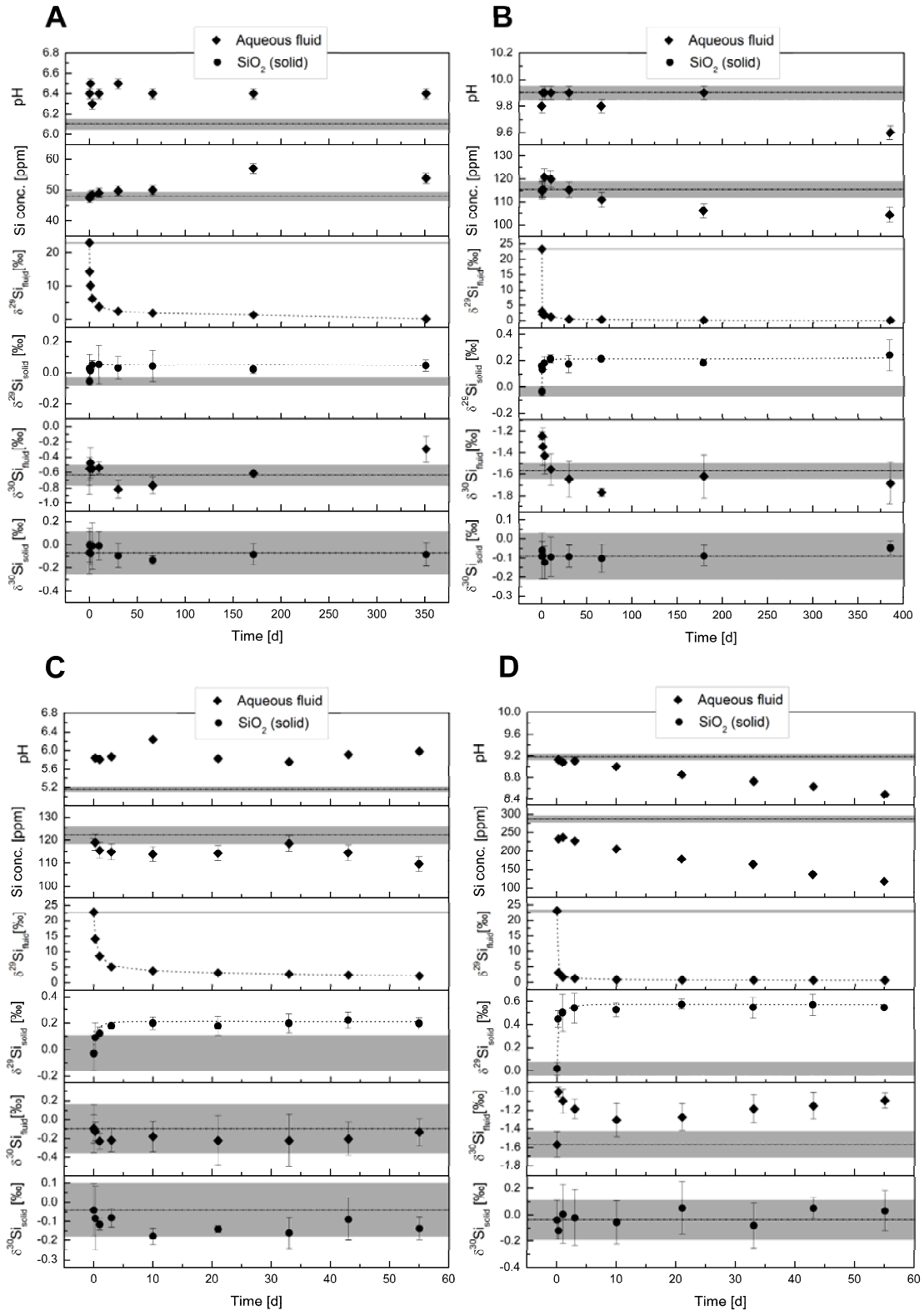

Fig. 5. Plots of pH, Si concentrations and isotopic compositions of solid and fluid phases as a function of time during the second step of each experimental series. The 2 S.D. uncertainties of data points are denoted by the error bars. Initial values are represented by dashed lines with their 2 S.D. error envelope shaded in grey. A) pH= 6.4 at 25 °C, B) pH= 9.9 at 25 °C, C) 5.8 at 75 °C, and D) 9.1 at 75 °C.

4.2.2 Chemical and isotopic evolution of the isotope exchange experiments

The temporal evolution of the pH, the bulk Si composition of the fluids, and the fluids and solids Si isotopic compositions during isotopic exchange step of all experimental series are provided in Fig. 5. The pH of the fluids remained close to constant during the experimental series other than during series run at pH 9.1 and 75°C, where the pH decreased somewhat. This decrease could be due to a loss of NH_4OH through evaporation over time from the reactors. Note that pH variations at alkaline conditions will alter the relative importance of the $H_3SiO_4^-$ versus $H_4SiO_4^0$ species in solution. As such the isotopic compositions of the final fluids of this high pH series were not considered in the determination of the equilibrium Si isotope fractionation factors given below. The dissolved Si concentrations remained close to constant during the pH ~6 experiments, but tended to decrease with time during the higher temperature experiments; this decrease is consistent with the observed decrease in pH, which tends to decrease amorphous silica solubility. The $\delta^{29}Si$ values of the fluids and solids mirror one another; in each case, the $\delta^{29}Si$ value of the ^{29}Si enriched fluid phase decreases rapidly at the beginning of each experimental series, while the $\delta^{29}Si$ value in the corresponding solid increases. Note that $\delta^{29}Si$ of the solids increase far less than the $\delta^{29}Si$ decreases in the fluid phase. This is due to the relative masses of Si in these phases; there is far more Si present in the solid than in the liquid phase in our experimental systems.

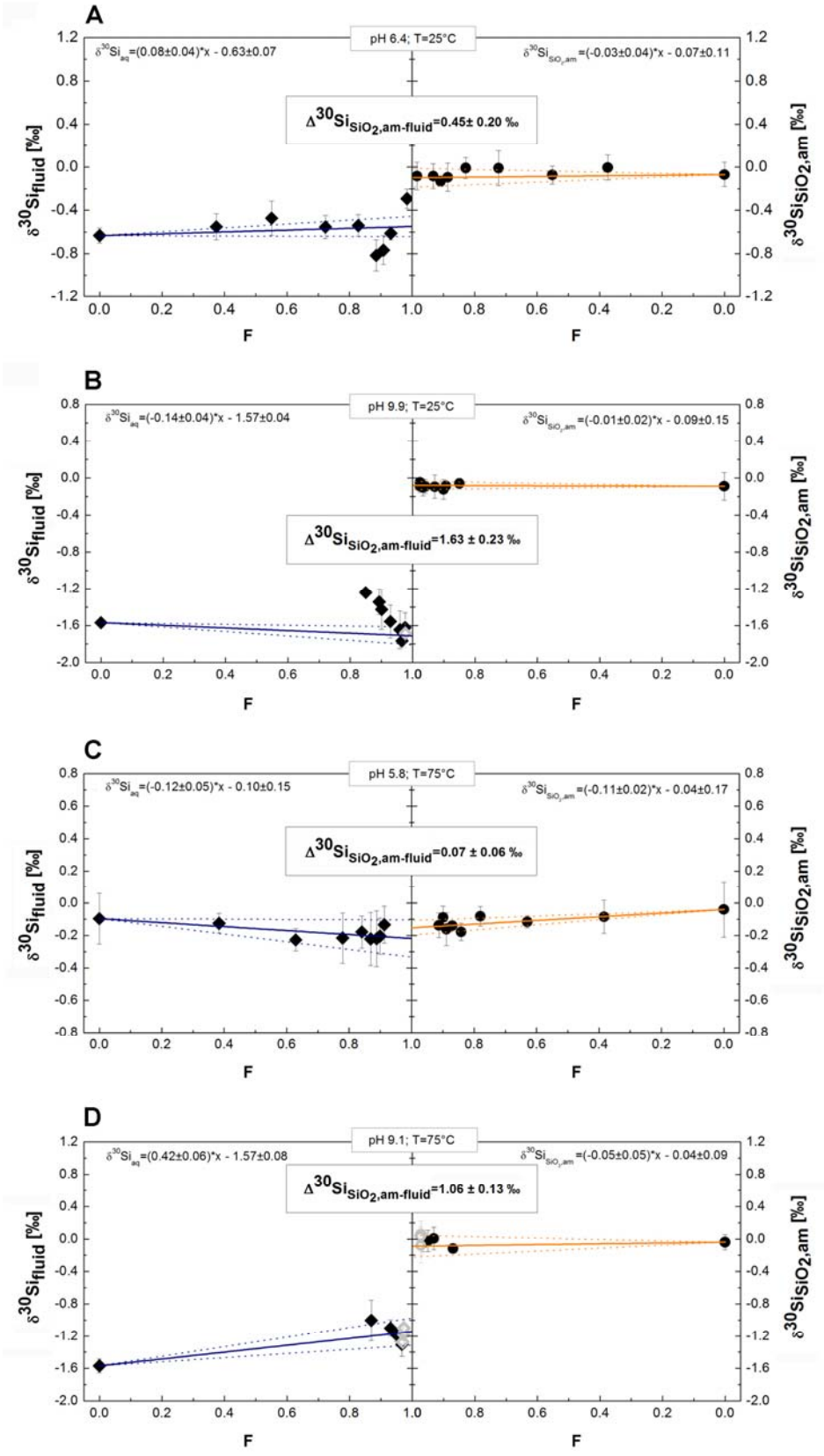

Fig. 6. Plots of the isotopic composition of the solid and fluid phases as a function of the degree of isotope exchange during the second step of each experimental series. A) pH= 6.4 at 25 °C , B) pH= 9.9 at 25 °C, C) 5.8 at 75 °C, and D) 9.1 at 75 °C. Excluded data from the fit are shown by grey symbols – see text.

Table 4. Average aqueous Si-speciation during the second step of each experimental series run in this study together with the resulting isotopic fractionation factors between solid and solution, solid and the $H_4SiO_4^0$ and $H_3SiO_4^-$ species, and between $H_3SiO_4^-$ and $H_4SiO_4^0$ species.

										Speciation						
Exp.	pH	Temperature	Si-conc.	$\Delta^{30}Si_{-SiO_2,am\text{-}fluid}$	2SD	$\Delta^{30}Si_{SiO_2,am\text{-}H_4SiO_4^0}$	2SD	$\Delta^{30}Si_{SiO_2,am\text{-}H_3SiO_4^-}$	2SD	$H_4SiO_4^0$	$H_3SiO_4^-$	$H_6(H_2SiO_4)_4^{2-}$	$H_2SiO_4^{2-}$	$H_4(H_2SiO_4)_4^{4-}$	$\Delta^{30}Si_{H_3SiO_4^-\text{-}H_4SiO_4^0}$	2SD
		[°C]	[mmol]	[‰]	[‰]	[‰]	[‰]	[‰]	[‰]	[%]	[%]	[%]	[%]	[%]	[‰]	[‰]
SibA	6.37	25	1.79	0.45	0.20	0.45	0.20			99.97	0.03	0.00	0.00	0.00		
SicB	9.84	25	4.05	1.63	0.23			2.79	0.15	47.49	48.20	3.99	0.07	0.25	-2.34	0.13
Sig75A	5.82	75	4.13	0.07	0.06	0.07	0.03			99.97	0.03	0.00	0.00	0.00		
Sik75B	9.11	75	8.48	1.06	0.13			2.28	0.07	54.16	43.78	2.05	0.00	0.01	-2.21	0.05

4.3. Silicon isotope fractionation factors

The *equilibrium* Si isotope fractionation factors, $\Delta_{eq}{}^{30}Si_{SiO_2,am\text{-}fluid}$, at the conditions of the four experimental series considered in this study were generated with the aid of Fig. 6 as described in section 2.3. The value of $\Delta_{eq}{}^{30}Si_{SiO_2,am\text{-}fluid}$, was estimated from the extrapolation to $F = 1$ of the solid lines drawn though the isotopic data shown in these figures. This fit was aided by the fact that these isotopic exchange reactions approached to within 90% of their final equilibrium compositions; the final values of F were 0.91 and 0.98 in these experimental series (see Table 2). A close correspondence can be seen between the isotopic data and these fits. The values of $\Delta_{eq}{}^{30}Si_{SiO_2,am\text{-}fluid}$ obtained from these fits are provided in Table 4 and vary with temperature and pH. Note that as mentioned above, the final few measurements of the experimental series performed at pH 9.9 and 25°C, and pH 9.1 and 75°C were excluded from the fit due to pH drift; their exclusion affected negligibly the retrieved values of $\Delta_{eq}{}^{30}Si_{SiO_2,am\text{-}fluid}$. The $\Delta_{eq}{}^{30}Si_{SiO_2,am\text{-}fluid}$ decreases by ~0.4‰ with increasing temperature from 25 to 75°C at pH 6. With increasing pH to ~9, however, the $\Delta_{eq}{}^{30}Si_{SiO_2,am\text{-}fluid}$ increases by 1.0 to 1.2 ‰.

The observed $\Delta_{eq}{}^{30}Si_{SiO_2,am\text{-}fluid}$ variation with pH can be attributed to the dependence of aqueous Si speciation on pH. The speciation of Si in the reactive fluids of each series is provided in Table 4. Aqueous Si was present almost exclusively as $H_4SiO_4^0$ in the pH ~6 experiments, but as much as 48% of dissolved Si in the pH ~9 experiments was present as the $H_3SiO_4^-$ species – see Fig. 1. In addition to the major aqueous Si species, $H_4SiO_4^0$ and $H_3SiO_4^-$, polymeric Si species represent <5 % of total Si speciation and are hence considered negligible. Therefore $H_4SiO_4^o$ and $H_3SiO_4^-$ are assumed to be 100 % of total Si-speciation in solution. Taking account of Eqns. (10) – (12) and the calculated speciation of Si in the aqueous phase in the experiments, the equilibrium Si isotope fractionation factors between amorphous silica and $H_4SiO_4^0$ or $H_3SiO_4^-$ ($\Delta_{eq}{}^{30}Si_{SiO_{2,am}m-H_4SiO_4^0}$ and $\Delta_{eq}{}^{30}Si_{SiO_{2,am}-H_3SiO_3^-}$) and between the species $H_3SiO_4^-$ and $H_4SiO_4^0$ ($\Delta_{eq}{}^{30}Si_{SiO_{2,am}m-H_4SiO_4^0}$) were determined at both 25° and 75°C. The resulting values are provided in Table 4.

4.4. Isotope exchange kinetics

The rate of attainment of isotopic equilibrium provides insight into the mechanism of isotope exchange. The temporal evolutions of the degree of isotope exchange, F, for the four experimental series in this study are shown in Fig 7. It can be seen that isotope exchange is relatively rapid during the first 10 days of each experimental series. After 10 days, the exchange reaction slows as the system approaches isotopic equilibrium. The curves in this figure were

generated using the first order rate law, Eqn. (16), to be consistent with the amorphous SiO_2 rate expression provided by Eqn. (3) to (7).

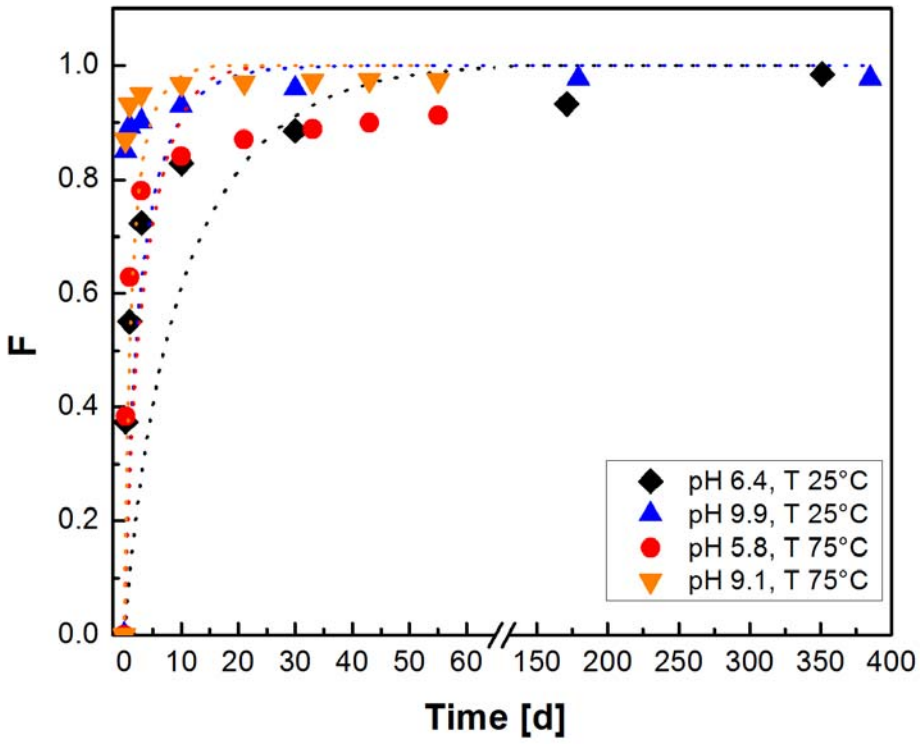

Fig. 7. The temporal evolution of the degree of isotopic exchange F during the four experimental series runs of this study. Dashed lines are generated assuming a first order rate law (Eqn. 16), using the dissolution rate constants from the amorphous silica dissolution rate experiments performed as the first step of each experimental series.

The rate constants used to generate these curves were those retrieved from the amorphous silica dissolution rate experiments run at the beginning of each series – see above and Table 3. It can be seen that the initial isotopic exchange rates shown in Table 5 are similar to- if not faster than- those of the bulk amorphous silica dissolution rates obtained from the first step of each experimental series. As isotopic equilibrium is approached, these isotope exchange rates become slow relative to that calculated from the bulk amorphous silica dissolution rates.

Table 5. Initial isotopic exchange rates, calculated from the first 10 days of isotope exchange based on a first order rate law.

		initial exchange	
Exp.	Si-conc. [mmol]	k_{exch} [1/s]	r_{exch} [mol/(m²*s)]
SibA	8.98	2.36×10^{-6}	6.64×10^{-13}
SicB	20.28	3.08×10^{-6}	2.71×10^{-12}
Sig75A	16.53	6.50×10^{-6}	3.63×10^{-12}
Sik75B	42.72	1.40×10^{-5}	2.20×10^{-11}

5. DISCUSSION

5.1. Silicon isotope fractionation between amorphous silica and aqueous solution

The equilibrium Si isotope fractionation factor between amorphous silica ($SiO_2 \cdot 0.32 H_2O$) and the aqueous solution determined in this study at 25°C and pH 6.4 where $H_4SiO_4^0$ accounts for 100% of dissolved silica is $\Delta_{eq}{}^{30}Si_{SiO_2,am\text{-}fluid} = \Delta_{eq}{}^{30}Si_{SiO_{2,am}-H_4SiO_4^0} =$ 0.45 ± 0.20 ‰. This value is identical, within uncertainty with those of Roerdink et al. (2015), who reported a $\Delta_{eq}{}^{30}Si_{SiO_2,am\text{-}fluid}$ of 0.0 ± 1.1 ‰ at 20 °C and 0.5 ± 0.6‰ at 35 °C for this system. Note that these former values were obtained at a pH of 8.5 from amorphous silica precipitation experiments using a surface kinetic model to correct for the effect of precipitation kinetics. Oelze et al. (2014) proposed a $\Delta_{eq}{}^{30}Si_{SiO_2,am\text{-}fluid}$ of -0.3 ‰ from experiments measuring the adsorption of silica onto gibbsite, and Oelze et al. (2015) proposed a $\Delta_{eq}{}^{30}S_{SiO_2,am\text{-}fluid}$ of around 0 ‰ based on amorphous silica precipitation experiments in the presence and absence of Al. The results of the present study, performed using the three-isotope method, which thereby verifies the attainment of isotopic equilibrium in the amorphous silica - aqueous solution system validates the results of these former studies. The three-isotope method was also adopted by Zheng et al. (2016) to assess the Si equilibrium fractionation factor between a Fe(III)-Si gel and an aqueous solution at pH 8. These authors report an equilibrium fractionation factor, $\Delta_{eq}{}^{30}Si_{SiO_2,am\text{-}fluid}$ of -2.3 ± 0.23 ‰. The differences between this result and those reported in the present study are likely attributable to the substantial presence of Fe(III) in the solid phase ($X_{Fe(III)}/X_{Si}$ = 0.5).

Many studies have shown that the absolute values of isotopic fractionation decreases as temperature increases (Urey, 1947; Bigeleisen, 1965; Schauble, 2004; Shahar et al., 2011; Huang et al., 2014). Such is also the case in the present study. At pH ~6 the $\Delta_{eq}{}^{30}Si_{SiO_2,am\text{-}fluid}$ decreases from 0.45 ± 0.20 ‰ to 0.07 ± 0.06 ‰ as temperature increases from 25 to 75 °C. At more alkaline conditions, these fractionation factors also depend on pH due to the formation of additional Si aqueous species. As the stability of these aqueous species depends on temperature, the explicit account of their speciation as a function of temperature is required to accurately estimate equilibrium Si isotope fractionation factors.

5.2. Isotope fractionation among Si aqueous species

The combination of fluid speciation and measured equilibrium fractionation factors at 2 different pH allows the determination of the equilibrium fractionation among amorphous silica, and the $H_4SiO_4^0$ and $H_3SiO_4^-$ aqueous species. The distinct equilibrium fractionation

factors among these species can be represented as $\Delta_{eq}{}^{30}Si_{SiO_{2,am}-H_4SiO_4^0}$, $\Delta_{eq}{}^{30}Si_{SiO_{2,am}-H_3SiO_3^-}$, and $\Delta_{eq}{}^{30}Si_{H_3SiO_4^- - H_4SiO_4^0}$, and are listed in Table 4. Dupuis et al. (2015) estimated $\Delta_{eq}{}^{30}Si_{quartz-H_4SiO_4^0}$ from *ab initio* calculations, obtaining 2.1± 0.20 ‰ for 25°C. This value is somewhat higher than that obtained between amorphous silica and this aqueous species in the present study, $\Delta_{eq}{}^{30}Si_{SiO_{2,am}-H_4SiO_4^0}$= 0.45 ± 0.20 ‰. This difference can be explained by the different structures of the solids. Quartz, with its continuous framework of SiO_4 tetrahedra, has an ordered structure, which is not the case of the partially hydrated amorphous silica used in this study. Therefore, the structural difference between quartz and aqueous $H_4SiO_4^0$ is more important than that between amorphous silica and aqueous $H_4SiO_4^0$. As such, quartz is expected to be enriched in ^{30}Si compared to amorphous silica.

The equilibrium Si isotope fractionation factor among the two major Si bearing aqueous Si species, $\Delta_{eq}{}^{30}Si_{H_3SiO_4^- - H_4SiO_4^0}$, was found in the present study to be -2.34 ± 0.13 ‰ and -2.21 ± 0.05 ‰ at 25° and 75°C, respectively. These values can be directly compared to the corresponding values determined using *ab initio* calculations. Dupuis et al. (2015) reported that at 25°C, $\Delta_{eq}{}^{30}Si_{H_3SiO_4^- - H_4SiO_4^0}$= -1.6 ± 0.30 ‰. In contrast, Fujii et al. (2015) reported that at 25°C, $\Delta_{eq}{}^{30}Si_{H_3SiO_4^- - H_4SiO_4^0}$= -3 ‰. The value generated in the present study falls between these calculated values.

The equilibrium Si isotope fractionation factor among the two major Si bearing aqueous species determined in the present study can also be compared to that measured by Fujii et al. (2015); this previous experimental study measured a 25°C $\Delta_{eq}{}^{30}Si_{H_3SiO_4^- - H_4SiO_4^0}$ equal to -3.5 ‰. The Fujii et al. (2015) study, however, took a different approach to determine this equilibrium fractionation factor than that of the present study. Their method relied on the purification of a Na_2SiO_4 solution at pH 9.4 by column chromatography using an anionic resin. The two dominant Si aqueous species were collected in different elutions. These elutions were then measured for their Si isotopic compositions. This approach allows running experiments at much lower Si concentrations than those of the present study since there is no need for the solutions to be in equilibrium with a solid Si-bearing phase. Note that at amorphous silica-aqueous fluid equilibrium at pH >9, there is a possibility of the formation of minor amounts of polynuclear Si bearing aqueous species (Dietzel, 2000) that could affect the measured equilibrium isotopic fractionation between amorphous silica and its coexisting aqueous fluid. The method used by Fuji et al. (2015) however, does not verify that isotopic equilibrium is

attained. Additionally, undefined fractionation may have occurred during the column separation by sorption of Si on the anionic resin (Fuji et al., 2015).

5.3. Kinetics of Si isotope exchange

The first part of each experimental series began by dissolving amorphous SiO_2 to equilibrium in its aqueous solution. The surface area normalized dissolution rates of these experiments were retrieved by fitting these data to the rate equations (4) to (7). The rates, reported in Table 3, range from 3.13 x 10^{-12} mol/m^2/s at 25°C and pH 6 to 1.24 x 10^{-10} mol/m^2/s at 75°C and pH 9; these rates increase with increasing temperature and increasing pH. They are similar to the dissolution rates of quartz obtained at corresponding temperature and pH conditions by Brady and Walther (1989), Berger et al. (1994), and Icenhower and Dove, (2000); these past reported values ranged from 10^{-12} to 10^{-13} mol/m²/s. Our values are also similar to the amorphous silica and the phytoliths dissolution rates of 10^{-12} and 3×10^{-12} mol/m²/s at 25°C, pH 5, and with comparable grain sizes reported by Plettnick et al. (1994) and Fraysse et al., (2006), respectively. In contrast, our rates are substantially slower than that of amorphous silica nanoparticles with a surface area of 232 m²/g at 25°C and pH 7 reported by Diedrich et al. (2012).

The rates of isotopic equilibration provide some insight into the process controlling isotopic equilibration. The variation of the degree of isotopic exchange (*F*) is plotted at a function of time in Fig 7. The curves through the data points in this figure were generated using the first order rate equation (Eqn. 16), to be consistent with the bulk dissolution rate equation. The rate constants used for these calculations were obtained from the dissolution of the amorphous silica during the first step of each experimental series. It can be seen in this figure that the curves are close to, but somewhat lower than the *F* values during the first 10 days of reaction, when isotope exchange has progressed to 80-95%. The isotope exchange rates tend to slow relative to that estimated using the corresponding bulk amorphous silica dissolution rates as the systems approach isotopic equilibrium beyond this *F* value. This behaviour suggests that the dominant rate-controlling mechanism of isotope equilibration in the present study over the first 10 to 20 days of the isotopic equilibration is the detachment and reattachment of silicic acid to and from the amorphous silica surface; note the system during this isotopic equilibration is at bulk chemical equilibrium such that this coupled attachment/detachment process does not result in net dissolution or precipitation. The observations of the post-material solids by SEM and TEM suggest that the grains are negligibly changed as a result of the isotope equilibration

process. Such observations favour the mechanism of an atomic-scale exchange of material at the solid-fluid interface rather than the recrystallization of the solid.

The observation that the isotopic exchange rates match closely the bulk dissolution rates measured during each isotopic exchange experimental series when F <80 to 95% suggests that Si transport rate within the amorphous silica grains in this study is relatively fast compared to the rate of detachment and attachment of SiO_2 at the surface for the bulk of the isotopic exchange process over this time period. This fast isotope exchange rate is likely due to the relatively small grain size of the amorphous SiO_2 used in the experiments; the average grain size of these particles was 21 ± 5 nm. Based on the unit cell dimension of quartz, which is ~ 5Å (Danielsson et al., 1976), it is likely that these grains are no more than ~40 unit cells across. In addition, the presence of water in the amorphous silica structure may facilitate the transport of Si into and out of these grains. Only after isotopic exchange has attained 80 to 90% of their equilibrium values do these exchange rates slow compared to bulk amorphous silica dissolution rates. This may indicate that the final equilibration of the isotope exchange reaction is becoming transport-limited near the end of each experimental series. Nevertheless, all experimental series performed in this study approached isotopic equilibrium within the 55 to 360 days of each experimental series. If the rapid rate of the total Si isotopic equilibration as observed here is also the case in natural ambient temperature systems, the preservation of original Si isotopic signatures in natural fine-grained amorphous SiO_2 materials may be rare.

5.4. Can Si fractionation be used as a paleo pH and temperature proxy?

Fujii et al. (2015) proposed the use of Si isotope fractionation as a proxy of seawater paleo-pH due to the pH-dependent concentration of the $H_3SiO_4^-$ and $H_4SiO_4^0$ species and the consequent variation of solid-aqueous fluid fractionation factors with pH. Seawater however has a pH of ~8 and thus mainly $H_4SiO_4^0$ will be present. As such, Si isotopes may be more useful for determining pH in more alkaline environments. Numerous such environments can be found in nature, for example in alkaline lakes (e.g. Mono Lake, California USA) or in mafic/ultramafic rocks. The results of this study confirm the possibility of using Si isotopic signatures in precipitated minerals as pH proxies of natural waters and provides the equilibrium Si isotope fractionation factors between amorphous SiO_2, the dominant SiO_2 phase precipitating at ambient conditions with its coexisting aqueous solution at different pH. The variation of amorphous SiO_2 – aqueous fluid fractionation factors determined as a function of pH at 25° and 75°C using Eqn. (12) and the equilibrium fractionation factors from this study are provided in

Fig 8. Although the variation of this fractionation factor with pH is substantially smaller than that of boron (Zeebe, 2005; Klochko et al., 2006; Noireaux et al., 2015), as the Si does not change its coordination in aqueous inorganic systems, it has the advantage of having a simpler and better-defined aqueous and solid speciation, potentially making it a more precise tool for constraining some paleo-pH values. Note, however, that the experiments presented in this study suggest that small (~20 nm) amorphous silica grains can rapidly equilibrate with its co-existing aqueous fluid in the laboratory. Moreover amorphous silica is hydrous; the presence of this water may facilitate Si transport within its structure. As such further work should be made on the kinetics of isotopic exchange as a function solid grain size and porosity, to assess the degree to which the Si isotope signatures of precipitated amorphous SiO_2 are preserved over geologic timeframes.

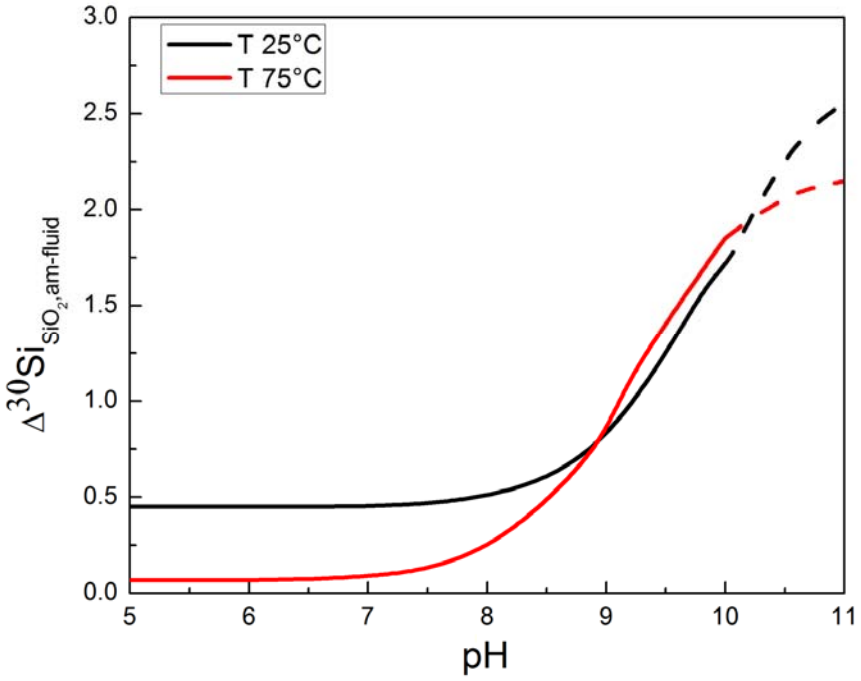

Fig. 8. Si equilibrium fractionation factors between amorphous silica and the fluid at 25°C and 75°C as a function of pH calculated using the Si equilibrium fractionation factors derived in the present study together with the aqueous speciation of Si shown in Fig 1. The curves in this figure are dashed at elevated pH as this calculation does not take into account polyatomic Si aqueous complexes, which may become important at these conditions.

The data obtained in this study not only show a variation in equilibrium Si isotope fractionation depending on solution pH, but also on solution temperature. The equilibrium Si isotope fractionation factor between amorphous SiO_2 and $H_4SiO_4^0$ at 75°C is significantly lower than that at ambient temperature. Si isotopic fraction becomes more important at lower temperatures. In Fig. 9, the equilibrium isotope fractionation factors of the present study at

neutral pH are extrapolated to 0 °C based on the polynomial function of Dupuis et al. (2015), showing that a fractionation of ~0.9 ‰ can be expected at this temperature. This conclusion is supported by the *ab initio* calculations of Dupuis et al. (2015) shown in Fig. 9, exhibiting a much stronger fractionation factor between quartz and $H_4SiO_4^0$ as temperature decreases. This relatively large fractionation factor at low temperature might explain the low $\delta^{30}Si$ signatures found in Banded Iron Formations (BIFS, Chakrabarti et al., 2012) and/or the $\delta^{30}Si$ variation of Archean cherts (Marin-Carbonne et al., 2012).

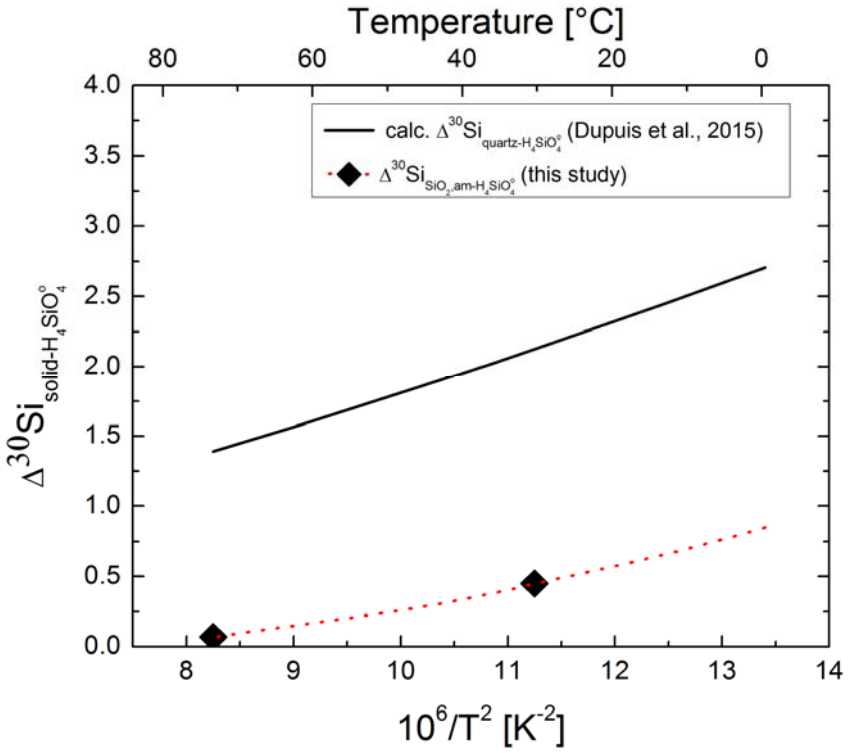

Fig. 9. Si equilibrium fractionation factors between quartz (Dupuis et al., 2015) and amorphous silica and $H_4SiO_4^o$ (this study) as a function of temperature. Red dotted describes extrapolated values.

6. CONCLUSIONS

The results presented in this study confirm the significance of aqueous silica speciation on equilibrium isotope fractionation between fluids and Si-bearing solids. The equilibrium fractionation factor between amorphous SiO_2 and its co-existing aqueous solution $\Delta_{eq}{}^{30}Si_{SiO_2,am\text{-}fluid}$ at 25°C is 0.45 ± 0.20 ‰ at pH 6 and 1.63 ± 0.23 ‰ at pH 9.9. Using these values and the distribution of the species in the aqueous solution, an equilibrium isotope fractionation value between $H_3SiO_4^-$ and $H_4SiO_4^\circ$, $\Delta_{eq}{}^{30}Si_{H_3SiO_4^- - H_4SiO_4^0}$= -2.34 ± 0.13 ‰ at 25°C was obtained. Such results suggest the possible use of the Si isotope signatures of precipitated Si bearing

minerals as a paleo pH proxy. Furthermore the Si isotopic fractionation between amorphous silica and its coexisting aqueous fluid decreases with increasing temperature, for example from 0.45 ± 0.20 ‰ at 25°C to 0.07 ± 0.06 ‰ at 75°C and pH 6. It follows that the Si isotopic compositions of precipitated amorphous silica may provide insight into the temperature of its formation.

This study also further validates the use of the three-isotope method as an effective means to determine both the rates of isotope exchange and equilibrium isotope fractionation factors. Such equilibrium fractionation factors facilitate greatly the interpretation of natural isotope signatures. The rates of isotope exchange determined by this approach may also provide new insight into both the mechanism of isotope exchange and the conditions at which mineral isotopic signatures are best preserved in natural systems.

ACKNOWLEDGEMENTS

This research was supported by ISONOSE a People Programme (Marie Curie Actions) of the European Unions' Seventh Framework Programme FP7/2017-2013/ under REA grant agreement n° [608069]. We thank Alain Castillo, Carole Causserand, and Manuel Henry from the Géosciences Environement Toulouse for BET measurements, and their assistance in the laboratories. Special thanks are extended to Merlin Méheut for providing precious information on *ab initio* calculation methods. The authors furthermore acknowledge Gwénaëlle Guittier from the Laboratoire de Génie Chimique (INP-ENSIACET) for TGA measurements, Philippe De Parseval, and Teresa Hungria from the Centre de MicroCaractérisation Raimond Castaing Toulouse, for SEM and TEM measurements, respectively. Josefine Buhk and Daniel Frick are thanked for their assistance with Si isotope measurements at GFZ. François-Xavier d'Abzac, Chiara Marieni, Moritz Lissner, Weiqiang Li, Giuseppe Saldi, and Martin Voigt are acknowledged for their helpful ideas, constructive discussions, and contributions to this work.

REFERENCES

Asael, D., Matthews, A., Oszczepalski, S., Bar-Matthews, M., Halicz, L., 2009. Fluid speciation controls of low temperature copper isotope fractionation applied to the Kupferschiefer and Timna ore deposits. Chem. Geol. 262, 147–158. https://doi.org/10.1016/j.chemgeo.2009.01.015

Balan, E., Noireaux, J., Mavromatis, V., Saldi, G.D., Montouillout, V., Blanchard, M., Pietrucci, F., Gervais, C., Rustad, J.R., Schott, J., Gaillardet, J., 2018. Theoretical isotopic fractionation between structural boron in carbonates and aqueous boric acid and borate ion. Geochim. Cosmochim. Acta 222, 117–129. https://doi.org/10.1016/j.gca.2017.10.017

Basile-Doelsch, I., Meunier, J.D., Parron, C., 2005. Another continental pool in the terrestrial silicon cycle. Nature 433, 399–402. https://doi.org/10.1038/nature03217

Beard, B.L., Handler, R.M., Scherer, M.M., Wu, L., Czaja, A.D., Heimann, A., Johnson, C.M., 2010. Iron isotope fractionation between aqueous ferrous iron and goethite. Earth Planet. Sci. Lett. 295, 241–250. https://doi.org/0.1016/j.epsl.2010.04.006

Berger, G., Cadore, E., Schott, J., Dove, P.M., 1994. Dissolution rate of quartz in lead and sodium electrolyte solutions between 25 and 300°C: Effect of the nature of surface complexes and reaction affinity. Geochim. Cosmochim. Acta 58, 541–551. https://doi.org/10.1016/0016-7037(94)90487-1

Bigeleisen, J., 1965. Chemistry of Isotopes: Isotope chemistry has opened new areas of chemical physics, geochemistry, and molecular biology. Science 147, 463–471. https://doi.org/10.1126/science.147.3657.463

Brady, P.V., Walther, J.V., 1989. Controls on silicate dissolution rates in neutral and basic pH solutions at 25°C. Geochim. Cosmochim. Acta 53, 2823–2830. https://doi.org/10.1016/0016-7037(89)90160-9

Brunauer, S., Emmett, P.H., Teller, E., 1938. Adsorption of Gases in Multimolecular Layers. J. Am. Chem. Soc. 60, 309–319. https://doi.org/10.1021/ja01269a023

Chakrabarti, R., Knoll, A.H., Jacobsen, S.B., Fischer, W.W., 2012. Si isotope variability in Proterozoic cherts. Geochim. Cosmochim. Acta 91, 187–201. https://doi.org/10.1016/j.gca.2012.05.025

Cole, D.R., Chakraborty, S., 2001. Rates and Mechanisms of Isotopic Exchange. Rev. Mineral. Geochem. 43, 83–223. https://doi.org/10.2138/gsrmg.43.1.83

Criss, R.., Gregory, R.., Taylor, H.., 1987. Kinetic theory of oxygen isotopic exchange between minerals and water. Geochim. Cosmochim. Acta 51, 1099–1108. https://doi.org/10.1016/0016-7037(87)90203-1

Danielsson, S., Grenthe, I., Oskarsson, å., 1976. A low-temperature apparatus for single-crystal diffractometry. The unit-cell dimension of α-quartz in the temperature range 86–298 K. J. Appl. Crystallogr. 9, 14–17. https://doi.org/10.1107/S0021889876010418

De La Rocha, C.L., Bescont, P., Croguennoc, A., Ponzevera, E., 2011. The silicon isotopic composition of surface waters in the Atlantic and Indian sectors of the Southern Ocean. Geochim. Cosmochim. Acta 75, 5283–5295. https://doi.org/10.1016/j.gca.2011.06.028

De La Rocha, C.L., Brzezinski, M.A., DeNiro, M.J., 2000. A first look at the distribution of the stable isotopes of silicon in natural waters. Geochim. Cosmochim. Acta 64, 2467–2477. https://doi.org/10.1016/S0016-7037(00)00373-2

De La Rocha, C.L., Brzezinski, M.A., DeNiro, M.J., Shemesh, A., 1998. Silicon-isotope composition of diatoms as an indicator of past oceanic change. Nature 395, 680–683. https://doi.org/10.1038/27174

Delstanche, S., Opfergelt, S., Cardinal, D., Elsass, F., André, L., Delvaux, B., 2009. Silicon isotopic fractionation during adsorption of aqueous monosilicic acid onto iron oxide. Geochim. Cosmochim. Acta 73, 923–934. https://doi.org/10.1016/j.gca.2008.11.014

Delvigne, C., Cardinal, D., Hofmann, A., André, L., 2012. Stratigraphic changes of Ge/Si, REE+Y and silicon isotopes as insights into the deposition of a Mesoarchaean banded iron formation. Earth Planet. Sci. Lett. 355–356, 109–118. https://doi.org/10.1016/j.epsl.2012.07.035

Demarest, M.S., Brzezinski, M.A., Beucher, C.P., 2009. Fractionation of silicon isotopes during biogenic silica dissolution. Geochim. Cosmochim. Acta 73, 5572–5583. https://doi.org/10.1016/j.gca.2009.06.019

Diedrich, T., Dybowska, A., Schott, J., Valsami-Jones, E., Oelkers, E.H., 2012. The Dissolution Rates of SiO 2 Nanoparticles As a Function of Particle Size. Environ. Sci. Technol. 46, 4909–4915. https://doi.org/10.1021/es2045053

Dietzel, M., 2000. Dissolution of silicates and the stability of polysilicic acid. Geochim. Cosmochim. Acta 64, 3275–3281. https://doi.org/10.1016/S0016-7037(00)00426-9

Ding, T.P., Gao, J.F., Tian, S.H., Wang, H.B., Li, M., 2011. Silicon isotopic composition of dissolved silicon and suspended particulate matter in the Yellow River, China, with

implications for the global silicon cycle. Geochim. Cosmochim. Acta 75, 6672–6689. https://doi.org/10.1016/j.gca.2011.07.040

Ding, T.P., Ma, G.R., Shui, M.X., Wan, D.F., Li, R.H., 2005. Silicon isotope study on rice plants from the Zhejiang province, China. Chem. Geol. 218, 41–50. https://doi.org/10.1016/j.chemgeo.2005.01.018

Ding, T.P., Tian, S.H., Sun, L., Wu, L.H., Zhou, J.X., Chen, Z.Y., 2008a. Silicon isotope fractionation between rice plants and nutrient solution and its significance to the study of the silicon cycle. Geochim. Cosmochim. Acta 72, 5600–5615. https://doi.org/10.1016/j.gca.2008.09.006

Ding, T.P., Zhou, J.X., Wan, D.F., Chen, Z.Y., Wang, C.Y., Zhang, F., 2008b. Silicon isotope fractionation in bamboo and its significance to the biogeochemical cycle of silicon. Geochim. Cosmochim. Acta 72, 1381–1395. https://doi.org/10.1016/j.gca.2008.01.008

Douthitt, C.., 1982. The geochemistry of the stable isotopes of silicon. Geochim. Cosmochim. Acta 46, 1449–1458. https://doi.org/10.1016/0016-7037(82)90278-2

Dupuis, R., Benoit, M., Nardin, E., Méheut, M., 2015. Fractionation of silicon isotopes in liquids: The importance of configurational disorder. Chem. Geol. 396, 239–254. https://doi.org/10.1016/j.chemgeo.2014.12.027

Fraysse, F., Pokrovsky, O.S., Schott, J., Meunier, J.-D., 2006. Surface properties, solubility and dissolution kinetics of bamboo phytoliths. Geochim. Cosmochim. Acta 70, 1939–1951. https://doi.org/10.1016/j.gca.2005.12.025

Frierdich, A.J., Beard, B.L., Scherer, M.M., Johnson, C.M., 2014. Determination of the Fe(II)aq–magnetite equilibrium iron isotope fractionation factor using the three-isotope method and a multi-direction approach to equilibrium. Earth Planet. Sci. Lett. 391, 77–86. https://doi.org/10.1016/j.epsl.2014.01.032

Frings, P.J., Clymans, W., Fontorbe, G., Gray, W., Chakrapani, G.J., Conley, D.J., De La Rocha, C., 2015. Silicate weathering in the Ganges alluvial plain. Earth Planet. Sci. Lett. 427, 136–148. https://doi.org/10.1016/j.epsl.2015.06.049

Fujii, T., Moynier, F., Blichert-Toft, J., Albarède, F., 2014. Density functional theory estimation of isotope fractionation of Fe, Ni, Cu, and Zn among species relevant to geochemical and biological environments. Geochim. Cosmochim. Acta 140, 553–576. https://doi.org/10.1016/j.gca.2014.05.051

Fujii, T., Pringle, E.A., Chaussidon, M., Moynier, F., 2015. Isotope fractionation of Si in protonation/deprotonation reaction of silicic acid: A new pH proxy. Geochim. Cosmochim. Acta 168, 193–205. https://doi.org/10.1016/j.gca.2015.07.003

Geilert, S., Vroon, P.Z., Roerdink, D.L., Van Cappellen, P., van Bergen, M.J., 2014. Silicon isotope fractionation during abiotic silica precipitation at low temperatures: Inferences from flow-through experiments. Geochim. Cosmochim. Acta 142, 95–114. https://doi.org/10.1016/j.gca.2014.07.003

Georg, R.B., Reynolds, B.C., Frank, M., Halliday, A.N., 2006. New sample preparation techniques for the determination of Si isotopic compositions using MC-ICPMS. Chem. Geol. 235, 95–104. https://doi.org/10.1016/j.chemgeo.2006.06.006

Georg, R.B., Reynolds, B.C., West, A.J., Burton, K.W., Halliday, A.N., 2007. Silicon isotope variations accompanying basalt weathering in Iceland. Earth Planet. Sci. Lett. 261, 476–490. https://doi.org/10.1016/j.epsl.2007.07.004

Georg, R.B., Zhu, C., Reynolds, B.C., Halliday, A.N., 2009. Stable silicon isotopes of groundwater, feldspars, and clay coatings in the Navajo Sandstone aquifer, Black Mesa, Arizona, USA. Geochim. Cosmochim. Acta 73, 2229–2241. https://doi.org/10.1016/j.gca.2009.02.005

Grasse, P., Ehlert, C., Frank, M., 2013. The influence of water mass mixing on the dissolved Si isotope composition in the Eastern Equatorial Pacific. Earth Planet. Sci. Lett. 380, 60–71. https://doi.org/10.1016/j.epsl.2013.07.033

He, H., Zhang, S., Zhu, C., Liu, Y., 2016. Equilibrium and kinetic Si isotope fractionation factors and their implications for Si isotope distributions in the Earth's surface environments. Acta Geochim. 35, 15–24. https://doi.org/10.1007/s11631-015-0079-x

Hemming, N.G., Hanson, G.N., 1992. Boron isotopic composition and concentration in modern marine carbonates. Geochim. Cosmochim. Acta 56, 537–543. https://doi.org/10.1016/0016-7037(92)90151-8

Hendry, K.R., Leng, M.J., Robinson, L.F., Sloane, H.J., Blusztjan, J., Rickaby, R.E.M., Georg, R.B., Halliday, A.N., 2011. Silicon isotopes in Antarctic sponges: an interlaboratory comparison. Antarct. Sci. 23, 34–42. https://doi.org/10.1017/S0954102010000593

Hendry, K.R., Robinson, L.F., 2012. The relationship between silicon isotope fractionation in sponges and silicic acid concentration: Modern and core-top studies of biogenic opal. Geochim. Cosmochim. Acta 81, 1–12. https://doi.org/10.1016/j.gca.2011.12.010

Holloway, J.M., Nordstrom, D.K., Böhlke, J.K., McCleskey, R.B., Ball, J.W., 2011. Ammonium in thermal waters of Yellowstone National Park: Processes affecting

speciation and isotope fractionation. Geochim. Cosmochim. Acta 75, 4611–4636. https://doi.org/10.1016/j.gca.2011.05.036

Huang, F., Wu, Z., Huang, S., Wu, F., 2014. First-principles calculations of equilibrium silicon isotope fractionation among mantle minerals. Geochim. Cosmochim. Acta 140, 509–520. https://doi.org/10.1016/j.gca.2014.05.035

Huang, T.-C., Tsai, F.-N., 1970. Kinetic studies on the isotopic exchange of calcium ion and calcium carbonate. J. Inorg. Nucl. Chem. 32, 17–31. https://doi.org/10.1016/0022-1902(70)80445-6

Icenhower, J.P., Dove, P.M., 2000. The dissolution kinetics of amorphous silica into sodium chloride solutions: effects of temperature and ionic strength. Geochim. Cosmochim. Acta 64, 4193–4203. https://doi.org/10.1016/S0016-7037(00)00487-7

Jiskra, M., Wiederhold, J.G., Bourdon, B., Kretzschmar, R., 2012. Solution Speciation Controls Mercury Isotope Fractionation of Hg(II) Sorption to Goethite. Environ. Sci. Technol. 46, 6654–6662. https://doi.org/10.1021/es3008112

Johnson, C.M., Skulan, J.L., Beard, B.L., Sun, H., Nealson, K.H., Braterman, P.S., 2002. Isotopic fractionation between Fe(III) and Fe(II) in aqueous solutions. Earth Planet. Sci. Lett. 195, 141–153. https://doi.org/10.1016/S0012-821X(01)00581-7

Kathrin Abraham, Opfergelt, S., Fripiat, F., Cavagna, A.-J., de Jong, J.T.M., Foley, S.F., André, L., Cardinal, D., 2008. δ30Si and δ29Si Determinations on USGS BHVO-1 and BHVO-2 Reference Materials with a New Configuration on a Nu Plasma Multi-Collector ICP-MS. Geostand. Geoanalytical Res. 32, 193–202. https://doi.org/10.1111/j.1751-908X.2008.00879.x

Klochko, K., Cody, G.D., Tossell, J.A., Dera, P., Kaufman, A.J., 2009. Re-evaluating boron speciation in biogenic calcite and aragonite using 11B MAS NMR. Geochim. Cosmochim. Acta 73, 1890–1900. https://doi.org/10.1016/j.gca.2009.01.002

Klochko, K., Kaufman, A.J., Yao, W., Byrne, R.H., Tossell, J.A., 2006. Experimental measurement of boron isotope fractionation in seawater. Earth Planet. Sci. Lett. 248, 276–285. https://doi.org/10.1016/j.epsl.2006.05.034

Li, W., Beard, B.L., Johnson, C.M., 2011. Exchange and fractionation of Mg isotopes between epsomite and saturated MgSO4 solution. Geochim. Cosmochim. Acta 75, 1814–1828. https://doi.org/10.1016/j.gca.2011.01.023

Li, Y., Ding, T., Wan, D., 1995. Experimental study of silicon isotope dynamic fractionation and its application in geology. Chin. J. Geochem. 14, 212–219. https://doi.org/10.1007/BF02842044

Marin-Carbonne, J., Chaussidon, M., Robert, F., 2012. Micrometer-scale chemical and isotopic criteria (O and Si) on the origin and history of Precambrian cherts: Implications for paleo-temperature reconstructions. Geochim. Cosmochim. Acta 92, 129–147. https://doi.org/10.1016/j.gca.2012.05.040

Marin-Carbonne, J., Robert, F., Chaussidon, M., 2014. The silicon and oxygen isotope compositions of Precambrian cherts: A record of oceanic paleo-temperatures? Precambrian Res. 247, 223–234. https://doi.org/10.1016/j.precamres.2014.03.016

Matsuhisa, Y., Goldsmith, J.R., Clayton, R.N., 1978. Mechanisms of hydrothermal crystallization of quartz at 250°C and 15 kbar. Geochim. Cosmochim. Acta 42, 173–182. https://doi.org/10.1016/0016-7037(78)90130-8

Matthews, A., Goldsmith, J.R., Clayton, R.N., 1983a. On the mechanisms and kinetics of oxygen isotope exchange in quartz and feldspars at elevated temperatures and pressures. Geol. Soc. Am. Bull. 94, 396. https://doi.org/10.1130/0016-7606(1983)94<396:OTMAKO>2.0.CO;2

Matthews, A., Goldsmith, J.R., Clayton, R.N., 1983b. Oxygen isotope fractionations involving pyroxenes: The calibration of mineral-pair geothermometers. Geochim. Cosmochim. Acta 47, 631–644. https://doi.org/10.1016/0016-7037(83)90284-3

Matthews, A., Goldsmith, J.R., Clayton, R.N., 1983c. Oxygen isotope fractionation between zoisite and water. Geochim. Cosmochim. Acta 47, 645–654. https://doi.org/10.1016/0016-7037(83)90285-5

Mavromatis, V., González, A.G., Dietzel, M., Schott, J., 2018. Zin isotope fractionation during inorganic precipitation of calcite - Towards a new pH proxy. Geochim. Cosmochim. Acta.

Noireaux, J., Mavromatis, V., Gaillardet, J., Schott, J., Montouillout, V., Louvat, P., Rollion-Bard, C., Neuville, D.R., 2015. Crystallographic control on the boron isotope paleo-pH proxy. Earth Planet. Sci. Lett. 430, 398–407. https://doi.org/10.1016/j.epsl.2015.07.063

Oelze, M., von Blanckenburg, F., Bouchez, J., Hoellen, D., Dietzel, M., 2015. The effect of Al on Si isotope fractionation investigated by silica precipitation experiments. Chem. Geol. 397, 94–105. https://doi.org/10.1016/j.chemgeo.2015.01.002

Oelze, M., von Blanckenburg, F., Hoellen, D., Dietzel, M., Bouchez, J., 2014. Si stable isotope fractionation during adsorption and the competition between kinetic and equilibrium isotope fractionation: Implications for weathering systems. Chem. Geol. 380, 161–171. https://doi.org/10.1016/j.chemgeo.2014.04.027

Opfergelt, S., Cardinal, D., André, L., Delvigne, C., Bremond, L., Delvaux, B., 2010. Variations of δ30Si and Ge/Si with weathering and biogenic input in tropical basaltic ash soils under monoculture. Geochim. Cosmochim. Acta 74, 225–240. https://doi.org/10.1016/j.gca.2009.09.025

Opfergelt, S., Cardinal, D., Henriet, C., André, L., Delvaux, B., 2006. Silicon isotope fractionation between plant parts in banana: In situ vs. in vitro. J. Geochem. Explor. 88, 224–227. https://doi.org/10.1016/j.gexplo.2005.08.044

Opfergelt, S., Georg, R.B., Delvaux, B., Cabidoche, Y.-M., Burton, K.W., Halliday, A.N., 2012. Silicon isotopes and the tracing of desilication in volcanic soil weathering sequences, Guadeloupe. Chem. Geol. 326–327, 113–122. https://doi.org/10.1016/j.chemgeo.2012.07.032

Opfergelt, S., Williams, H.M., Cornelis, J.T., Guicharnaud, R.A., Georg, R.B., Siebert, C., Gislason, S.R., Halliday, A.N., Burton, K.W., 2017. Iron and silicon isotope behaviour accompanying weathering in Icelandic soils, and the implications for iron export from peatlands. Geochim. Cosmochim. Acta 217, 273–291. https://doi.org/10.1016/j.gca.2017.08.033

Parkhurst, D.L., Appelo, C.A.J., 2013. Description of input and examples for PHREEQC version 3—A computer program for speciation, batch-reaction, one-dimensional transport, and inverse geochemical calculations. U.S. Geological Survey Techniques and Methods, book 6, chap. A43, p. 497.

Platzner, I.T. (Itzhak T., Habfast, K., Walder, A.J., Goetz, A., 1997. Modern isotope ratio mass spectrometry, Chemical analysis. J. Wiley, Chichester ; New York.

Plettnick, S., Chou, L., Wollast, R., 1994. Kinetics and mechanisms of dissolution of silica at room temperature and pressure. Mineral. Mag. 58A.

Pogge von Strandmann, P.A.E., Opfergelt, S., Lai, Y.-J., Sigfússon, B., Gislason, S.R., Burton, K.W., 2012. Lithium, magnesium and silicon isotope behaviour accompanying weathering in a basaltic soil and pore water profile in Iceland. Earth Planet. Sci. Lett. 339–340, 11–23. https://doi.org/10.1016/j.epsl.2012.05.035

Poitrasson, F., 2017. Silicon Isotope Geochemistry. Rev. Mineral. Geochem. 82, 289–344. https://doi.org/10.2138/rmg.2017.82.8

Pokrovski, G.S., Schott, J., 1998. Experimental study of the complexation of silicon and germanium with aqueous organic species: implications for germanium and silicon transport and Ge/Si ratio in natural waters. Geochim. Cosmochim. Acta 62, 3413–3428. https://doi.org/10.1016/S0016-7037(98)00249-X

Pokrovsky, O.S., Reynolds, B.C., Prokushkin, A.S., Schott, J., Viers, J., 2013. Silicon isotope variations in Central Siberian rivers during basalt weathering in permafrost-dominated larch forests. Chem. Geol. 355, 103–116. https://doi.org/10.1016/j.chemgeo.2013.07.016

Reddy, T.R., Frierdich, A.J., Beard, B.L., Johnson, C.M., 2015. The effect of pH on stable iron isotope exchange and fractionation between aqueous Fe(II) and goethite. Chem. Geol. 397, 118–127. https://doi.org/10.1016/j.chemgeo.2015.01.018

Reynolds, B., Frank, M., Halliday, A., 2006. Silicon isotope fractionation during nutrient utilization in the North Pacific. Earth Planet. Sci. Lett. 244, 431–443. https://doi.org/10.1016/j.epsl.2006.02.002

Rimstidt, J.D., Barnes, H.L., 1980. The kinetics of silica-water reactions. Geochim. Cosmochim. Acta 44, 1683–1699. https://doi.org/10.1016/0016-7037(80)90220-3

Riotte, J., Meunier, J.-D., Zambardi, T., Audry, S., Barboni, D., Anupama, K., Prasad, S., Chmeleff, J., Poitrasson, F., Sekhar, M., Braun, J.-J., 2018a. Processes controlling silicon isotopic fractionation in a forested tropical watershed: Mule Hole Critical Zone Observatory (Southern India). Geochim. Cosmochim. Acta 228, 301–319. https://doi.org/10.1016/j.gca.2018.02.046

Riotte, J., Sandhya, K., Prakash, N.B., Audry, S., Zambardi, T., Chmeleff, J., Buvaneshwari, S., Meunier, J.-D., 2018b. Origin of silica in rice plants and contribution of diatom Earth fertilization: insights from isotopic Si mass balance in a paddy field. Plant Soil 423, 481–501. https://doi.org/10.1007/s11104-017-3535-z

Roerdink, D.L., van den Boorn, S.H.J.M., Geilert, S., Vroon, P.Z., van Bergen, M.J., 2015. Experimental constraints on kinetic and equilibrium silicon isotope fractionation during the formation of non-biogenic chert deposits. Chem. Geol. 402, 40–51. https://doi.org/10.1016/j.chemgeo.2015.02.038

Russell, W.A., Papanastassiou, D.A., Tombrello, T.A., 1978. Ca isotope fractionation on the Earth and other solar system materials. Geochim. Cosmochim. Acta 42, 1075–1090. https://doi.org/10.1016/0016-7037(78)90105-9

Ryan, B.M., Kirby, J.K., Degryse, F., Harris, H., McLaughlin, M.J., Scheiderich, K., 2013. Copper speciation and isotopic fractionation in plants: uptake and translocation mechanisms. New Phytol. 199, 367–378. https://doi.org/10.1111/nph.12276

Savage, P.S., Armytage, R.M.G., Georg, R.B., Halliday, A.N., 2014. High temperature silicon isotope geochemistry. Lithos 190–191, 500–519. https://doi.org/10.1016/j.lithos.2014.01.003

Savage, P.S., Georg, R.B., Williams, H.M., Halliday, A.N., 2013. The silicon isotope composition of the upper continental crust. Geochim. Cosmochim. Acta 109, 384–399. https://doi.org/10.1016/j.gca.2013.02.004

Schauble, E.A., 2004. Applying Stable Isotope Fractionation Theory to New Systems. Rev. Mineral. Geochem. 55, 65–111. https://doi.org/10.2138/gsrmg.55.1.65

Schindelin, J., Arganda-Carreras, I., Frise, E., Kaynig, V., Longair, M., Pietzsch, T., Preibisch, S., Rueden, C., Saalfeld, S., Schmid, B., Tinevez, J.-Y., White, D.J., Hartenstein, V., Eliceiri, K., Tomancak, P., Cardona, A., 2012. Fiji: an open-source platform for biological-image analysis. Nat. Methods 9, 676–682. https://doi.org/10.1038/nmeth.2019

Schott, J., Mavromatis, V., Fujii, T., Pearce, C.R., Oelkers, E.H., 2016. The control of carbonate mineral Mg isotope composition by aqueous speciation: Theoretical and experimental modeling. Chem. Geol. 445, 120–134. https://doi.org/10.1016/j.chemgeo.2016.03.011

Schuessler, J.A., von Blanckenburg, F., 2014. Testing the limits of micro-scale analyses of Si stable isotopes by femtosecond laser ablation multicollector inductively coupled plasma mass spectrometry with application to rock weathering. Spectrochim. Acta Part B At. Spectrosc. 98, 1–18. https://doi.org/10.1016/j.sab.2014.05.002

Shahar, A., Hillgren, V.J., Young, E.D., Fei, Y., Macris, C.A., Deng, L., 2011. High-temperature Si isotope fractionation between iron metal and silicate. Geochim. Cosmochim. Acta 75, 7688–7697. https://doi.org/10.1016/j.gca.2011.09.038

Shahar, A., Young, E.D., Manning, C.E., 2008. Equilibrium high-temperature Fe isotope fractionation between fayalite and magnetite: An experimental calibration. Earth Planet. Sci. Lett. 268, 330–338. https://doi.org/10.1016/j.epsl.2008.01.026

Steinhoefel, G., von Blanckenburg, F., Horn, I., Konhauser, K.O., Beukes, N.J., Gutzmer, J., 2010. Deciphering formation processes of banded iron formations from the Transvaal and the Hamersley successions by combined Si and Fe isotope analysis using UV femtosecond laser ablation. Geochim. Cosmochim. Acta 74, 2677–2696. https://doi.org/10.1016/j.gca.2010.01.028

Truesdale, V.W., LeCorre, P., 1975. Manuel d'analyse des sels nuritifs dans l'eau de mer: Utilisation de L'autoanalyzer II technicon (r). Université de Bretagne occiendtale, France.

Urey, H.C., 1947. The thermodynamic properties of isotopic substances. J. Chem. Soc. Resumed 562. https://doi.org/10.1039/jr9470000562

van den Boorn, S.H.J.M., van Bergen, M.J., Vroon, P.Z., de Vries, S.T., Nijman, W., 2010. Silicon isotope and trace element constraints on the origin of ~3.5Ga cherts: Implications for Early Archaean marine environments. Geochim. Cosmochim. Acta 74, 1077–1103. https://doi.org/10.1016/j.gca.2009.09.009

Welch, S.A., Beard, B.L., Johnson, C.M., Braterman, P.S., 2003. Kinetic and equilibrium Fe isotope fractionation between aqueous Fe(II) and Fe(III). Geochim. Cosmochim. Acta 67, 4231–4250. https://doi.org/10.1016/S0016-7037(03)00266-7

Wischmeyer, A.G., De La Rocha, C.L., Maier-Reimer, E., Wolf-Gladrow, D.A., 2003. Control mechanisms for the oceanic distribution of silicon isotopes. Glob. Biogeochem. Cycles 17, n/a-n/a. https://doi.org/10.1029/2002GB002022

Wu, L., Percak-Dennett, E.M., Beard, B.L., Roden, E.E., Johnson, C.M., 2012. Stable iron isotope fractionation between aqueous Fe(II) and model Archean ocean Fe–Si coprecipitates and implications for iron isotope variations in the ancient rock record. Geochim. Cosmochim. Acta 84, 14–28. https://doi.org/10.1016/j.gca.2012.01.007

Yin, R., Feng, X., Wang, J., Li, P., Liu, J., Zhang, Y., Chen, J., Zheng, L., Hu, T., 2013. Mercury speciation and mercury isotope fractionation during ore roasting process and their implication to source identification of downstream sediment in the Wanshan mercury mining area, SW China. Chem. Geol. 336, 72–79. https://doi.org/10.1016/j.chemgeo.2012.04.030

Young, E.D., Galy, A., Nagahara, H., 2002. Kinetic and equilibrium mass-dependent isotope fractionation laws in nature and their geochemical and cosmochemical significance. Geochim. Cosmochim. Acta 66, 1095–1104. https://doi.org/10.1016/S0016-7037(01)00832-8

Zambardi, T., Poitrasson, F., 2011. Precise Determination of Silicon Isotopes in Silicate Rock Reference Materials by MC-ICP-MS. Geostand. Geoanalytical Res. 35, 89–99. https://doi.org/10.1111/j.1751-908X.2010.00067.x

Zeebe, R.E., 2005. Stable boron isotope fractionation between dissolved B(OH)3 and B(OH)4−. Geochim. Cosmochim. Acta 69, 2753–2766. https://doi.org/10.1016/j.gca.2004.12.011

Zhang, J., Quay, P.D., Wilbur, D.O., 1995. Carbon isotope fractionation during gas-water exchange and dissolution of CO2. Geochim. Cosmochim. Acta 59, 107–114. https://doi.org/10.1016/0016-7037(95)91550-D

Zheng, X.-Y., Beard, B.L., Reddy, T.R., Roden, E.E., Johnson, C.M., 2016. Abiologic silicon isotope fractionation between aqueous Si and Fe(III)–Si gel in simulated Archean

seawater: Implications for Si isotope records in Precambrian sedimentary rocks. Geochim. Cosmochim. Acta 187, 102–122. https://doi.org/10.1016/j.gca.2016.05.012

Ziegler, K., Chadwick, O.A., Brzezinski, M.A., Kelly, E.F., 2005a. Natural variations of δ30Si ratios during progressive basalt weathering, Hawaiian Islands. Geochim. Cosmochim. Acta 69, 4597–4610. https://doi.org/10.1016/j.gca.2005.05.008

Ziegler, K., Chadwick, O.A., White, A.F., Brzezinski, M.A., 2005b. δ30Si systematics in a granitic saprolite, Puerto Rico. Geology 33, 817. https://doi.org/10.1130/G21707.1

Table A

Exp.	Temperature [°C]	Time [d]	pH	Si-conc. [ppm]	Si-conc. [mmol/kg]
SibA:					
	25	0	8.7	0.00	0.00
	25	1	5.5	2.71	0.10
	25	4	6.6	14.75	0.53
	25	7	6.0	23.07	0.82
	25	13	6.8	32.80	1.17
	25	19	6.6	39.02	1.39
	25	27	6.7	44.18	1.57
	25	37	6.4	46.69	1.66
	25	47	6.2	44.40	1.58
SicB:					
	25	0	10.2	0.00	0.00
	25	1	10.2	58.18	2.07
	25	4	10.2	104.08	3.71
	25	8	10.2	114.93	4.09
	25	16	10.2	124.72	4.44
	25	26	10.1	125.19	4,46
	25	50	10.2	114.73	4.08
	25	66	10.1	118.66	4.22
Sig75A:					
	75	0	5.9	0.00	0.00
	75	1	6.4	41.12	1.46
	75	4	6.5	87.67	3.12
	75	19	5.8	108.03	3.85
	75	23	5.7	107.12	3.81
	75	29	5.8	115.10	4.10
	75	33	5.7	114.91	4.09
	75	41	5.7	116.65	4.15
	75	69	5.7	117.35	4.18
Sik75B:					
	75	0	9.25	0.00	0.00
	75	1	10.02	148.71	5.29
	75	3	9.4	236.23	8.41
	75	8	9.9	231.37	8.24
	75	14	9.3	264.18	9.41
	75	22	9.3	257.85	9.18
	75	37	9.3	257.35	9.16

Table B

sample	Temp. [°C]	run time [d]	S_{BET} [m^2/g]	grain size [nm]	m_{H2O} [wt %]	chemical formula
SibA 8	25	351	137.1	20.86	9.4	$SiO_2 \cdot 0.33\ H_2O$
SicB 8	25	385	164.1	20.69	8.6	$SiO_2 \cdot 0.34\ H_2O$
Sig75A 8	75	55	171.7	19.60	8.1	$SiO_2 \cdot 0.28\ H_2O$
Sik75B 6	75	33	119.0	n.a.	7.5	$SiO_2 \cdot 0.32\ H_2O$

TABLE CAPTION ELECTRONIC SUPPLEMENT

Table A: Temporal evolution of dissolved Si concentration and pH during equilibration of the initial Si-free reactive fluids with the pre-treated amorphous silica.

Table B: Summary of the measured characteristics of the reacted solids collected after the longest duration experiment for the experiments at 25°C and pH 5.8 at 75°C. Longest reacted powder available at time of analysis at pH 9.1 and 75°C after 33 days.